Dynamic regulation of gonadal homeostasis across the lifespan of the naturally short-lived African turquoise killifish

Bryan B. Teefy[1], Ari Adler[1], Alan Xu[1,2], Param Priya Singh[3], Bérénice A. Benayoun[1,2,4,5,6,*]

[1] Leonard Davis School of Gerontology, University of Southern California, Los Angeles, CA 90089, USA.

[2] Molecular and Computational Biology Department, USC Dornsife College of Letters, Arts and Sciences, Los Angeles, CA 90089, USA.

[3] Department of Genetics, Stanford University, Stanford, CA, USA

[4] Biochemistry and Molecular Medicine Department, USC Keck School of Medicine, Los Angeles, CA 90089, USA.

[5] USC Norris Comprehensive Cancer Center, Epigenetics and Gene Regulation, Los Angeles, CA 90089, USA.

[6] USC Stem Cell Initiative, Los Angeles, CA 90089, USA.

[*] Corresponding author (berenice.benayoun@usc.edu).

Abstract

Although germline cells are considered to be functionally “immortal”, both the germline and supporting somatic cells in the gonad within an organism will experience aging. With increased age at parenthood, the age-related decline in reproductive success has become an important biological issue for an aging population. However, molecular mechanisms underlying reproductive aging across sexes in vertebrates remain poorly understood. To decipher molecular drivers of vertebrate gonadal aging across sexes, we perform longitudinal characterization of the gonadal transcriptome throughout lifespan in the naturally short-lived African turquoise killifish *(Nothobranchius furzeri)*. By combining mRNA-seq and small RNA-seq, we characterize the aging gonads of young adult, middle-aged, and old fish. We analyze changes in transcriptional patterns of genes, transposable elements (TEs), and piRNAs. We find that testes seem to undergo only marginal changes during aging. In contrast, in middle-aged ovaries, the timepoint associated with peak female fertility in this species, PIWI pathway components are transiently downregulated, TE transcription is elevated, and piRNA levels generally decrease, suggesting that egg quality may already be declining at middle-age. Furthermore, we show that piRNA ping-pong biogenesis declines steadily with age in ovaries, while it is maintained in aging testes. To our knowledge, this dataset represents the most comprehensive transcriptomic dataset for vertebrate gonadal aging. This resource also highlights important pathways that are regulated during reproductive aging in either ovaries or testes, which could ultimately be leveraged to help restore aspects of youthful reproductive function.

Introduction

In much of the industrialized world, parental age is increasing making fertility-related challenges associated with later-life childbearing increasingly relevant (Bertoldo et al., 2020; Kenny et al., 2013). In humans, oocyte quality begins to rapidly degrade around 30 years old while menopause, the irreversible loss of female fertility, occurs around 50 years old (Alberts et al., 2013; Finch, 2014). In contrast, while male fertility gradually declines with age, complete loss of testicular function is not a feature of male reproductive aging (Gunes et al., 2016). Mammals, as well as birds, are exceptional among vertebrates as these groups produce a finite supply of oocytes before or shortly after birth ensuring that any species that lives long enough should eventually deplete its oocytes, although the starting supply of oocyte greatly outnumbers the final number of oocytes that will be ovulated (Mira, 1998). However, there are many other mechanisms that influence reproductive decline, such as neuroendocrine aging, that occur in both sexes and are widely conserved among vertebrates (Perheentupa and Huhtaniemi, 2009). Thus, leveraging a tractable vertebrate model organism to understand molecular mechanisms underlying reproductive aging will provide important insights into lifelong regulation of reproductive function.

To study reproductive aging, we examined the impact of aging on testes and ovaries in the African Turquoise Killifish *Nothobranchius furzeri*, the shortest-lived vertebrate that can be bred in captivity, with a lifespan of about 4-6 months (Hu and Brunet, 2018). The turquoise killifish evolved this short lifespan in response to their unique lifecycle, which revolves around the formation of ephemeral ponds of water (Kim et al., 2016). Depending on the specific species, killifish can become sexually mature as early as two weeks post-hatching, although most killifish become sexually mature around 4-5 weeks of age, the fastest known time to sexual maturation of any vertebrate (Naumann and Englert, 2018; Vrtilek et al., 2018). Killifish are asynchronous breeders, and upon sexual maturity, females continuously undergo oogenesis and lay eggs, typically on a daily basis (Terzibasi Tozzini and Cellerino, 2020). Importantly, we and others have helped establish a key functional genomics toolkit for this species, making it a uniquely tractable experimental model to decipher molecular mechanisms driving aspects of aging (Harel et al., 2016; Reichwald et al., 2015; Valenzano et al., 2015; Valenzano et al., 2011; Willemsen et al., 2020).

An emerging facet of vertebrate aging is the reactivation of transposable elements (TEs) with aging in somatic tissues (Chen et al., 2016; De Cecco et al., 2013; LaRocca et al., 2020; Simon et al., 2019; Yang et al., 2022). However, whether TEs also transcriptionally activate within the aging gonad, which is uniquely protected from spurious TE mobilization by the PIWI-piRNA pathway, has been largely unexplored in a vertebrate system. The PIWI pathway is an Argonaute-based small RNA pathway that maintains germline genomic integrity by antagonizing the mobilization of transposable elements (TEs) through complementary RNA

base-pairing and TE RNA target degradation during gametogenesis and embryogenesis. PIWI family proteins bind 24-35 nucleotide (nt) PIWI-interacting RNAs, or piRNAs, which are complementary to or derived from TEs. piRNAs are expressed primarily in the gonad and are distinctly larger than miRNAs (Czech and Hannon, 2016; Mani and Juliano, 2013). Once bound to an RNA target, PIWI proteins cleave the RNA target precisely 10 nts from the 5' end of the complementary piRNA (Czech and Hannon, 2016; Mani and Juliano, 2013). To date, most studies examining the impact of aging on the PIWI pathway have focused on invertebrate model organisms, such as the fly *Drosophila melanogaster* (Lin et al., 2020; Sousa-Victor et al., 2017; Yamashiro and Siomi, 2018). For instance, Piwi expression is required to suppress TE expression, reduce DNA damage, and maintain intestinal stem cell lineages in the aging Drosophila midgut (Sousa-Victor *et al.*, 2017). In the fly ovary, age-related decline in *Piwi* expression in the cells of the germline stem cell niche results in a transposon de-repression and a loss of germline stem cells (GSCs) (Lin *et al.*, 2020). In contrast to the germline stem cell niche, the expression of PIWI pathway components in whole Drosophila egg chambers increases with age, although this is not associated with any global changes in TE expression (Erwin and Blumenstiel, 2019). Whether TEs are derepressed with age in the vertebrate gonad and whether TE expression is modulated by age-related PIWI dynamics remains unknown. Thus, it will be important to determine whether PIWI regulation (and concomitant TE control) in the aging gonad may influence reproductive aging.

Here, we characterize aging African turquoise killifish ovaries and testes using mRNA-seq and small RNA-seq in young adults (5 weeks), middle-age (10 weeks) and old (15 weeks) animals using the GRZ inbred lab strain. We show that TE and piRNA expression are affected primarily by the nature of the gonad (*i.e.* testis vs. ovary), although age-related dynamics exist. Interestingly, ovaries seem to undergo more age-related changes compared to testes, with most differential regulation occurring at middle-age, notably in terms of TE expression and PIWI pathway activity. Thus, our dataset provides a unique window into the transcriptional trajectory of gonadal aging, suggesting that important age-related events may impact egg quality as early as middle-age.

Results

Lifespan, reproductive, and transcriptomic landscapes of the aging gonad in the African turquoise killifish

To understand how gonads are affected during aging in a vertebrate model organism, we performed a study of ovarian and testicular landscapes throughout aging in African turquoise killifish from the GRZ strain (**Fig. 1A**). In our housing conditions (see Methods), 15 weeks correspond to ~90% survival for both female and male animals (**Fig. 1B; Supplementary Table S1A**), although GRZ females lived significantly longer than males in our husbandry conditions (p = 0.002, log Rank test; see Methods) (**Fig. 1B**). To determine the effect of aging on the vertebrate gonadal transcriptomic landscape, we collected ovaries and testes from N = 5 GRZ female and male African turquoise killifish at three different time points post-hatching: young adulthood (5 weeks; onset of fertility), middle age/peak female fecundity (10 weeks), and old age (15 weeks; before the dramatic population survival decrease) (**Fig. 1A**). In the turquoise killifish GRZ strain, fecundity peaks around 10-12 weeks (Zak and Reichard, 2021), corresponding to the middle-age time point that we selected. Only samples with intact RNA (RIN >7) were processed further to eliminate biases linked to RNA degradation, yielding 14 female samples and 12 male samples, leaving at least 4 samples per biological group (**Fig. S1A**). We performed (i) mRNA transcriptome characterization (*i.e.* mRNA-seq using polyA selection), analyzing both transcriptional patterns of genes and transposable elements [TEs], and (ii) small-RNA transcriptome characterization (*i.e.* small RNA-seq), focusing on piRNAs, the germline-specific class of small RNAs of the PIWI pathway (**Fig. 1A** and **S1A**).

To globally visualize the similarity of the transcriptomic landscapes of aging ovaries and testes at multiple levels of regulation, we used principal component analysis [PCA] (**Fig. 1C-E**). PCA analysis of genic mRNA, TE mRNA, and TE-targeting piRNA expression revealed that the main source of variation [PC1] corresponded to gonadal identity (*i.e.* ovary vs. testis), although animal age also weakly separated samples for mRNA and piRNA cluster (but not TEs) transcription on PC2 (**Fig. 1C-E**). Notably, despite genomic TE content being a fixed feature for the species, we observed clear sex-dimorphism in the transcriptional landscape of TEs and associated piRNAs in the turquoise killifish gonads. These observations are consistent with deeply sex-dimorphic transcriptional programs in the gonad at the level of mRNAs, TEs and small RNAs, and are consistent with a recent study in young *Drosophila* ovaries and testes (Chen et al., 2021). Separately, we analyzed the ovarian and testicular transcriptomes to uncover potential sex-specific transcriptional trajectories with aging (**Fig. S1B-G**). Middle-aged female expression data clustered distinctly for all analyzed RNA species in PC1 (**Fig. S1B-D**). This observation may reflect the outsized contribution of a transcriptional program associated with oogenesis, or fertility more broadly, to the expression profiles of all

RNA species assayed at this timepoint. Intriguingly, female piRNA expression data segregated most strongly by age, suggesting that the small RNA program in the ovary is most sensitive to aging (**Fig. S1D**). In contrast, the male transcriptomic data did not cluster strongly by age (**Fig. S1E-G**). Together, our observations suggest that testicular identity and function are more stable in response to organismal aging compared to those of ovary. Interestingly, our results are reminiscent of a microarray analysis of gonadal aging in mice, where ovaries underwent substantially more transcriptional changes with aging than testes (Sharov et al., 2008). Together, our data suggests unique changes in the transcriptional landscapes of ovaries versus testes throughout aging.

Aging differentially impacts gene expression in turquoise killifish ovaries and testes

Since aging is often a non-linear process, at least in somatic tissues (Baumgart et al., 2016; Rosenberg et al., 2021), we decided to determine differential gene expression with aging within the DEseq2 framework using a likelihood ratio testing [LRT] approach, so as to unbiasedly identify patterns of differential gene expression in ovary and testis aging (Love et al., 2014). To note, since LRT can be overly lenient (Core, 2021), we used a stringent False Discovery Rate [FDR] threshold of FDR <1e-6 to identify differentially expressed transcripts. Significantly regulated transcripts were then assigned to patterns using 'degPatterns' from the 'DEGreport' R package (Pantano, 2022), which uses hierarchical clustering of gene expression to identify shared significant patterns of expression among differentially expressed genes in an unsupervised fashion. This unbiased approach detected four major differential patterns corresponding to transcripts whose expression is (a) transiently down at middle-age, (b) transiently up at middle-age, (c) monotonously down with age, or (d) monotonously up with age (**Fig. 2A-B**, **3A**, **S2A** and **S3A**; **Supplementary Table S2A-B,D**). For reading convenience, we label these age-related patterns of differential expression hereafter as (a), (b), (c) and (d) whenever they arise from the unsupervised 'degPatterns' clustering. Intriguingly, we noted the majority of differentially expressed genes showed transient changes at middle-age in both ovaries and testes (respectively 1931 out of 2041, and 578 out of 603 differentially expressed genes), rather than linear trends with age. This trend suggests that most of the transcriptional variation in gonadal gene expression occurs at middle-age when fertility, at least in females, is at its peak. This observation is interesting, because it suggests that gonadal biology is already substantially impacted in middle-age healthy animals.

Next, we asked which biological functions were associated with each of these gene expression patterns with gonadal aging. For this purpose, we performed Gene Ontology [GO] Enrichment Analysis for each age-regulated pattern in ovaries and testes (Falcon and Gentleman, 2007) (**Fig. 2C**, **3B**, **S2B** and **S3B**; **Supplementary Table S3A-F**). First, we examined enrichment for terms in the "Biological Process" GO category (**Fig. 2C**, **3B**;

Supplementary Table S3A,D). Interestingly, genes downregulated in middle-aged ovaries were enriched most strongly for "piRNA metabolic process" (*i.e.* pattern a; GO:0034587; **Fig. 2C**; **Supplementary Table S3A**). Specifically, genes transcriptionally downregulated in middle-age ovaries include the genes encoding both effector PIWI proteins (*i.e.* the turquoise killifish homologs to human *PIWIL1* and *PIWIL2*), is consistent with overall decreased TE processing capacity. To note, as seen in **Supplementary Table S1C**, genes belonging to the "piRNA metabolic process" GO terms are, as expected, robustly expressed in killifish gonads throughout life. Intriguingly, in zebrafish, the gene encoding PIWIL1, the primary catalytic protein of the PIWI pathway, is expressed most highly in developing germline stem cells before expression decreases in more mature oocytes (Liu et al., 2022), which could indicate a higher ratio of mature oocytes to developing germline stem cells in middle-aged killifish ovaries compared to young and old ovaries. Thus, downregulation of PIWI-related genes at mid-age may be related to differences in mature oocytes content. Alternatively, this may also suggest that there is a relaxation of piRNA-mediated TE expression control in ovaries at middle-age in the African turquoise killifish (see below). Other terms enriched for genes downregulated in middle-age ovaries were largely related to egg maturation and egg-specific processes (*e.g.* zona pellucida and regulation of acrosome reaction; **Fig. 2C**), consistent with the notion that ovarian function (and oocyte quality) may have already started to decline at middle-age in the African turquoise killifish.

Genes that were upregulated in middle-aged ovaries were enriched for terms related to RNA metabolism, consistent with conserved importance of maternally deposited RNAs in oocytes (*i.e.* pattern b; **Fig. 2C**). Genes that were linearly downregulated with age in the ovaries were enriched for terms relating to extracellular matrix organization (*i.e.* pattern c; **Fig. 2C**). Finally, genes that were upregulated with age in the ovaries included those involved in immune responses and ion homeostasis (*i.e.* pattern d; **Fig. 2C**), which may relate to overall increases in inflammation with aging that has been observed in somatic tissues (Benayoun et al., 2019). Increased expression of inflammatory genes has also been observed in the transcriptome of aging mouse ovaries (Sharov *et al.*, 2008). We also performed a similar functional enrichment analysis using terms from the "Cellular Component" (**Fig. S2B; Supplementary Table S3B**). and "Molecular Function" (**Supplementary Table S3C**).GO categories, with largely consistent trends.

In aging testes, we observed the emergence of a similar trend, with most differential genes being regulated at middle-age (*i.e.* patterns a and b), and few genes linearly regulated with aging (*i.e.* patterns c and d; **Fig. 3A**; **Supplementary Table S3D**). Genes transiently downregulated at middle-age were enriched for terms relating to vascular development (pattern a; **Fig. 3B**). This observation suggests that the vasculature of the testis may be actively remodeled, consistent with known unique vascular requirements for testicular function

(Sargent et al., 2015). Genes transiently upregulated at middle-age included those involved in spermatogenesis, *e.g.* "axoneme assembly" and "cilium movement", consistent with peak spermatogenesis potentially occurring at this stage (pattern b; **Fig. 3B**). Lastly, genes that were downregulated linearly with age were heavily enriched for steroid biosynthesis related terms, suggestive of a steady decline in steroid biosynthesis in the aging gonad (pattern c; **Fig. 3B**). Interestingly, this transcriptional downregulation of steroid biosynthesis genes is consistent with a recent mass-spectrometry study that detected significantly decreased levels of sex-steroids in the testes of aging turquoise killifish (Dabrowski et al., 2020). “Cellular component” analysis again corroborated the GO “Biological Process” analysis, especially with regards to sperm-related terms being upregulated at middle-age (**Fig. S3B**; **Supplementary Table S3E**). Terms downregulated at middle-age included those associated with heterochromatin and extracellular vesicles, while terms downregulated linearly with age are enriched for mitochondrial and collagen related terms (**Fig. S3B, Table S3E**).

Together, our results show that the African turquoise killifish gonadal transcriptional landscapes are broadly remodelled at middle-age, highlighting the need to include middle-age time points in such analyses to get a full view of age-related trajectories. Notably, the largest changes in gene expression seem to align with the window of peak fertility and egg production in this species, suggesting that egg quality may start declining at middle-age despite high egg output.

Transposon expression is age- and sex-dependent in the turquoise killifish gonad

Next, we asked whether control of TE transcription may be impacted during gonadal aging in the turquoise killifish. Indeed, accumulating evidence has shown that TE expression tends to increase with age in somatic tissues across species (Benayoun *et al.*, 2019; Bravo et al., 2020; Chen *et al.*, 2016; De Cecco *et al.*, 2013; LaRocca *et al.*, 2020; Simon *et al.*, 2019; Yang *et al.*, 2022). Although TE control is especially important in the germline to maintain genome stability throughout generations, whether TE expression escapes control in gonadal tissues with vertebrate aging has not yet been investigated. Interestingly, a recent genomic analysis of several species of African killifishes suggests that the shorter-lived killifish species have been accumulating TEs in their genomes, suggesting that short-lived/annual killifish species, such as the African turquoise killifish, may not efficiently repress germline TE activity throughout life (Cui et al., 2020).

To determine whether global changes in TE expression can indeed occur in aging killifish gonads, we first analyzed what proportion of mapped reads in our mRNA-seq dataset were derived from TE sequences (**Fig. 4A-B**). TE-derived sequences represented approximately 7-11% of reads in turquoise killifish ovaries and testes (**Fig. 4B**). Interestingly, global levels of TE-derived mRNA sequences were stable between young and middle-aged

ovaries, but significantly dipped in old ovaries, whereas they tended to proportionally increase with age in testes (**Fig. 4B**). Such a pattern may reflect the process of gametogenesis, wherein the epigenome is repatterned, resulting in TE reactivation (Ben Maamar et al., 2021), despite the expected antagonizing effects of the PIWI pathway on TE expression in the germline.

Next, we asked whether TE transcription was changed with aging in ovaries and testes at the level of each subfamily. We identified differentially expressed TE transcripts using our mRNA-seq analysis pipeline (FDR < 1e-6, as above; **Fig. 4A,C,D** and **S4A-B; Supplementary Table S4A-B**). Similar to our differential gene expression analysis, we observed that most significant changes in TE expression levels occurred in middle-aged gonads (*i.e.* patterns a and b; **Fig. 4C,D** and **S4A,B**). In the ovary, 6 TEs were downregulated only at middle-age (pattern a), and 248 TEs were specifically upregulated at middle-age (pattern b; **Fig. 4C** and **S4A**). These age-regulated TEs seem to belong to families broadly representative of the overall turquoise killifish genomic TE content, with a predominance of LINE sequences, suggestive of general relaxation of TE control (**Fig. 4C,D**). Interestingly, this timepoint coincides with the functional enrichment for "piRNA metabolic process" for genes downregulated in middle-age ovaries (**Fig. 2C**). Thus, the transcriptional upregulation of TEs in the middle age ovary may reflect a unfavorable reactivation of certain TE species in response to the transient decline in PIWI pathway activity. Such an increase in TE transcription, even in the context of mature oocytes, is expected to be deleterious to oocyte health (Malki et al., 2014). In the aging testes, only 25 TEs passed our differential expression threshold (FDR < 1e-6), and they were all upregulated at middle-age (pattern b; **Fig. 4D** and **S4B**). A burst of TE transcription in middle-age gonads could reflect peak fertility and gamete output, where a higher proportion of germ cells are undergoing epigenetic repatterning to yield increased numbers of mature gametes. Alternatively, increased TE transcription may reflect a relaxation of genome surveillance mechanisms, ultimately leading to decreased gamete quality and survivability.

piRNAs and the PIWI pathway activity are regulated throughout life in turquoise killifish gonads

Thus far, we have found that: (i) genes encoding the key components of the PIWI pathways are robustly expressed throughout life in turquoise killifish ovaries and testes (**Supplementary Table S1C**; **Fig. 5A**), (ii) PIWI pathway genes are downregulated in ovaries at middle-age (**Fig. 5A** and **2C**), and (iii) transcription of TEs is globally regulated with gonadal aging (**Fig. 4B**), with several TE subfamilies transcriptionally specifically upregulated in middle-age ovaries and, to a lesser extent, middle-age testes (**Fig. 4C,D**). Thus, we reasoned that underlying changes in piRNA abundances throughout aging may drive changes in TE transcriptional levels.

To analyze PIWI pathway activity in ovaries and testes throughout turquoise killifish life, we generated small RNA sequencing libraries from the same samples used for mRNA-seq (**Fig. 1A, S1A**). We leveraged these libraries to annotate piRNA clusters and evaluate piRNA expression throughout life in the African turquoise killifish gonads. First, to computationally isolate piRNAs from our small RNA-seq library, we used a size filter of 24-35 nucleotides, which was previously shown to efficiently capture piRNAs and separate them from miRNAs (Gong et al., 2018; Huang et al., 2019) (**Fig. S5A**). Consistent with the resulting reads deriving from piRNAs, the resultant nucleotide composition showed the expected strong 1U bias in both types of gonads (Thomson and Lin, 2009) (**Fig. 5B**). In addition, these piRNA-derived reads seemed to arise from 222 unique piRNA clusters in the turquoise killifish genome, as identified by Protrac (Rosenkranz and Zischler, 2012). Importantly, the predicted TE content of the identified piRNA clusters is remarkably reflective of the annotated genomic TE content (**Fig. 5C**), consistent with the co-evolution between the TE invasion of the genome and the genomic defense against TE activity. In contrast to mice, in which ovarian piRNAs are rare and the PIWI pathway is broadly believed to be non-essential (Watanabe et al., 2008), turquoise killifish ovaries seem to express the components of PIWI pathway throughout life and are replete with piRNAs. This may be the result of continuous oocyte production in the killifish ovary since PIWI is required during oogenesis (Ketting, 2011; Roovers et al., 2015; Thomson and Lin, 2009).

Since piRNAs will align almost exclusively to TE sequences, we modelled piRNA abundance dynamics by performing differential expression analysis on TEs using counts from the piRNAs mapping to TE sequences embedded within the genome. This approach enables us to distinguish which TE species are differentially targeted by the PIWI pathway in turquoise killifish gonads as a function of age. As piRNA biogenesis is expected to at least partially be a response to TE activity, TE-specific piRNA counts should positively correlate with expressed TE species. Indeed, we observed a strong positive correlation between the mRNA levels of TEs and the abundance of cognate piRNAs in each biological group (Spearman Rank correlation Rho ≥ 0.66; **Fig. S5B,C**). Similar to transcriptional patterns observed in our genic and TE data, the bulk of differential piRNA expression occurred at middle-age in ovarian tissue (pattern a; **Fig. 5D** and **S5D**; **Supplementary Table S5A**). However, mirroring the TE transcriptional changes where many TE species were <u>upregulated</u> in the middle-age ovaries (**Fig. 4C**), the majority of differentially abundant piRNAs were <u>downregulated</u> at middle-age in the ovaries (**Fig. 5D**), consistent with downregulation of the PIWI pathway genes (**Fig. 2C** and **5A**). Importantly, there was significant overlap between TEs that were specifically upregulated in middle-age ovaries and TEs targeted by piRNAs with decreased piRNA abundance in middle age ovaries (p = 9.08E-3 in Fisher's exact test; **Fig. 5F**), consistent with the notion of a partial relaxation of piRNA-mediated TE repression in middle-age ovaries. Testis piRNA

expression was not as strongly regulated with age as compared to that of ovaries, with few age-regulated piRNA species, most of which showed increased expression with age (pattern d; **Fig. 5E** and **S5E**).

Ping-Pong activity declines with age in oocytes, remains stable in testes

In the presence of a particular TE mRNA, the PIWI pathway initializes catalytic degradation of the TE transcript guided by TE-complementary "primary" piRNA sequences, which triggers the production of additional "secondary" piRNA sequences that specifically target the active TE sequence (Czech and Hannon, 2016). This mechanism of piRNA synthesis through amplification of piRNA populations corresponding to actively transcribed TEs is known as "ping-pong" biogenesis (Czech and Hannon, 2016) (**Fig. 6A**). Effectively, ping-pong biogenesis is an adaptive mechanism by which the PIWI pathway defends the germline against active TE threats (Czech and Hannon, 2016). Due to the annealing requirements between primary piRNA sequences, target TE mRNAs, and TE-derived secondary piRNAs, a signature of ping-pong biogenesis is a 10 bp overlap between the 5' ends of opposite orientation piRNAs (Wang et al., 2015) (**Fig 6A** and **S6A-B**). This ping-pong biogenesis mechanism can be measured globally or at the level of a specific TE sequence.

We first used the PPmeter tool from the Protrac software suite to globally measure ping-pong biogenesis rates in each biological group (Jehn et al., 2018) (**Fig. 6B**). This tool calculates the instances of 10 bp overlaps out of every million overlap pairs assayed to report the relative fraction of reads engaged in active ping-pong within a given piRNA sequencing library. We used this tool for each biological replicate with 100 bootstraps and report the median values in each biological sample over bootstrap samples (**Fig. 6B**). In parallel, we also used an independent method in which, for each consensus TE sequence, we computed Z_{10} scores, a standard measure of ping-pong activity defined as the Z-score of the 10 bp overlap frequencies between opposite orientation piRNAs within a 20bp window (Han et al., 2015; Vandewege et al., 2022). For each replicate, we took the median Z_{10} score over all detected TE sequences to assess ping-pong at a global scale (**Fig. 6C**). Convincingly, both orthogonal methods revealed a steady decrease of the piRNA population participating in ping-pong biogenesis with aging in the ovaries, whereas this fraction remained relatively stable in the testes (**Fig. 6C**). The age-related decline in ovarian ping-pong activity may be related to a decrease in piRNA processing component expression starting at middle age (**Fig. 5A**). This trend could result in a decrease in the ability of the PIWI pathway to control TE transcription levels with ovarian aging. Alternatively, this steady decrease with aging in ovarian ping-pong biogenesis may reflect the interplay of (i) a decreased efficiency of the PIWI pathway at middle-age (**Fig. 2C**, **5A**), and (ii) an overall decrease of TE transcription levels in old ovaries (**Fig. 4B**). Meanwhile, the observed steady global ping-pong rates in testes are consistent with

relatively stable TE and piRNA expression dynamics relative to ovaries that we observed (**Fig. 4D, 5E**).

We were curious whether ping-pong biogenesis may be differentially regulated for each consensus TE sequence. For this purpose, we further examined the consensus TE Z_{10} data at the consensus TE transcript level. We used an ANOVA-based analysis to determine which TEs have differential levels of ping-pong activity as measured by Z_{10} scores with aging in ovaries and testes (**Fig. 6D-F** and **S6C-D**). Then, TEs with significant age-related changes in ping-pong biogenesis were clustered into patterns, similar as before using the 'degPatterns' paradigm (**Fig. 2A**, **6D**). This analysis identified TEs with ping-pong biogenesis levels corresponding to previously described patterns b, c and d. In addition, it identified 2 significant patterns for TEs with decreased ping-pong biogenesis at middle-age (the pattern previously designated as (a)): (a_1) with maximal ping-pong biogenesis in the young gonad, or (a_2) maximal ping-pong biogenesis in the old gonad. Interestingly, most of the TEs showing differential ping-pong levels in the ovaries showed significantly decreased ping-pong with aging (pattern c; **Fig. 6E** and **S6C**), consistent with the global ping-pong trends (**Fig. 6B,C**). In the testes, 82 TEs show differential ping-pong scores but without a clear global age-related trend, possibly reflecting a more robust PIWI activity throughout life (**Fig. 6F** and **S6D**). In summary, multiple methods of analysis show ping-pong activity progressively wanes in the aging ovary, but remains steady in the testes which may be reflective of respective gametogenesis rates in the female versus male gonads throughout life.

Discussion

A resource for the study of reproductive aging in vertebrates

The germline is considered an immortal cell lineage but the somatic cells that comprise and support the germline are affected by aging. In this study, we examined how aging affects the female and male gonads of a naturally short-lived vertebrate species, the African turquoise killifish. To our knowledge, this dataset is the largest 'omic' dataset evaluating vertebrate ovarian and testicular aging and will represent a unique resource for reproductive aging research. With our inclusion of a middle-aged time point, in addition to young adult and old ages, this dataset enables the discovery of dynamic and non-linear patterns of regulation, thus helping understand gonadal aging trajectories in addition to just the endpoint of gonadal aging. Indeed, we found that many key events, including those relating to TE transcriptional regulation and piRNA pathway regulation, are most salient at middle-age in ovaries, rather than undergoing linear changes with age. To note, our observations differ from reports in *Drosophila* egg chambers, in which PIWI-related genes were upregulated during aging though global TE expression levels remained largely stable (Erwin and Blumenstiel, 2019). Importantly, our observations that the aging ovarian transcriptome is more impacted than the testicular transcriptome are consistent with previous microarray studies of mouse gonadal aging (Sharov *et al.*, 2008).

A unique crosstalk between piRNA biogenesis and TE activity in the aging vertebrate gonad

We characterized TE expression and PIWI pathway behavior throughout life in turquoise killifish ovaries and testes. Importantly, we found that the PIWI pathway controls TE expression in the gonads throughout the turquoise killifish lifespan. Age-related fertility decline is common across many metazoans (Jones et al., 2014). The turquoise killifish is no exception to this rule, with female fertility generally declining after middle-age, especially in females (Zak and Reichard, 2021). For both sexes, fertility peaks around the middle-age timepoint used in this study (Zak and Reichard, 2021). Interestingly, this timepoint coincided with the largest changes in TE- and piRNA related events in both sexes. This may correspond to a period of increasing gametogenesis in which epigenetic modifications are globally removed from germ cells prior to repatterning. Such epigenetic erasure would provide a means of "escape" for TEs in the form of transcription. Since the females are asynchronous spawners and continuously produce oocytes, we might expect that, like in males, TE transcription may reflect gamete production output.

Overall, even in this short-lived species, the PIWI pathway seems to broadly keep gonadal TE transcription stable at the global transcriptomic level (**Fig. 4B**), although there is clear regulatory variation depending on specific TE sequences. This relatively controlled transcriptional output for TE loci seems to contrast with reports of global transcriptional

derepression of TE sequences in aging somatic tissues (Bravo *et al.*, 2020; De Cecco *et al.*, 2013). When expressed, TEs can cause DNA damage and/or initiate innate immune responses due to their intrinsic similarity to viruses (Simon *et al.*, 2019). This contrast between TE activity in germline/somatic tissues is especially interesting considering that non-aging taxa (*e.g. Hydra*, *Planaria*) can express PIWI in somatic stem cells (Sahu et al., 2017; Schaible et al., 2015; Teefy et al., 2020). This suggests that looser TE control may drive aspects of aging, especially in the soma, whereas tighter TE control is crucial to allow the emergence of non-aging states, such as those found in the germline.

Dynamic TE control in the aging African turquoise killifish ovary

If the turquoise killifish piRNA metabolism dynamics are similar to those of zebrafish, the depletion of PIWI at middle-age could merely indicate a higher proportion of mature oocytes (Liu *et al.*, 2022). Alternatively, increased TE expression in middle-aged ovaries (and thus decreased TE control) may be a symptom of decreased oocyte quality before fertility starts to decline, suggesting that reproductive aging may precede organismal decline. Finally, it is possible that such a transient relaxation of TE control in middle-age ovaries for the turquoise killifish may have adaptative value. Indeed, allowing some level of TE mobilization in the germline through tunable activity of the PIWI pathway could help ensure adequate levels of genetic diversity in a species with naturally small populations due to its unique ecology. Consistently, annual killifish, like *Nothobranchius furzeri*, have much higher genomic TE content than non-annual killifish species that do not experience such extreme population bottlenecks from seasonal aquatic habitat desiccation (Cui *et al.*, 2020).

TEs have long been appreciated in plant biology for their contribution to genetic diversity and are now appreciated sources of genetic diversity and drivers of speciation in animals (Akagi et al., 2013; Bariah et al., 2020; Belyayev, 2014; Catlin and Josephs, 2022; Chen et al., 2020; Gonzalez et al., 2010; McClintock, 1984). In line with the hypothesis that relaxed germline TE restriction may enhance population-level genetic diversity is our observation that ping-pong rate in killifish ovaries decreases steadily with age. This age-related PIWI behavior could support a population facing severe bottlenecks by first generating many healthier (but less genetically diverse) progeny during young adulthood. Subsequently, with females still breeding at a more advanced age, reduced PIWI pathway activity could help generate a more genetically diverse pool of progeny that could improve genetic diversity for the long-term adaptability of the local population.

In summary, our data supports the notion that even a short-lived species such as the African turquoise killifish can maintain adequate TE silencing in germline-containing tissues throughout life, likely due to the activity of the PIWI pathway. The impact of fluctuations in TE

transcription and PIWI pathway activity, especially in ovarian tissues, remains an open question. Understanding disruptions to gonadal genomic regulatory networks during aging will be crucial to define strategies to preserve or prolong reproductive fitness with aging.

Material and methods

African turquoise killifish husbandry

African turquoise killifish were raised according to gold standard procedures (Dodzian et al., 2018). To decrease risks of aggression, adult fish were single housed in 2.8L tanks on a recirculating aquatics system manufactured by Aquaneering Inc. System water parameters were as follows: temperature: 29°C; pH: 7.3; conductance: 670-750 µS; ammonia and nitrite: 0ppm and Nitrate: ~15 ppm. Adult fish were fed twice per day with Hikari Freeze Dried Bloodworms 4-6 hours apart, and live *Artemia* once per day. Fry were reared in system water incubated at 28°C, then placed on the recirculating system starting at 2 weeks post hatch. Fry were fed live *Artemia* exclusively until 4 weeks post hatch. The fish facility was kept on a light/dark cycle of 13/11 hours (lights on 9am-10pm). The fish were euthanized by immersion in 1.5 g/L of Tricaine MS-222 dissolved in system water followed by decapitation. All fish were euthanized between 2 and 4 pm to minimize circadian effects. All husbandry conditions and experimental procedures were approved by the University of Southern California (USC) IACUC. Animal care and animal experimentation were performed in accordance with IACUC approved protocols for *Nothobranchius furzeri at* the University of Southern California (approved protocols *20879* and *21023*).

Lifespan data collection

Lifespan data was derived from historical data in our colony collected 2019-2022. Time from hatching to humane endpoint/euthanasia or natural death was recorded as killifish lifespan. All lifespan data reported here is derived from single-housed fish to limit death or injuries linked with frequent fighting in this species.

RNA extraction and sequencing

Ovaries and testes were dissected from 5-week-old, 10-week-old, and 15-week-old turquoise killifish (N = 5 per group) and flash-frozen on dry ice. Total RNA was extracted from flash-frozen gonads by homogenizing using Trizol (Thermo Fisher, 15596018) and Lysing Matrix D tubes (MP Biomedicals, 11422420) on a BeadBug 6 microtube homogenizer (Millipore Sigma, Z742683) for 2 rounds of 30 seconds at 3500 rpms. RNA was assayed for quality at the USC Genome Core using the Agilent Bioanalyzer total RNA assay, and only high-quality RNA samples (RIN > 7) were selected for further processing to avoid RNA degradation related biases. Due to poor RNA quality, samples for three males (one from each age group) and one 15-week female were eliminated at this stage. RNA samples were sent to Novogene Corporation (USA) for library construction and sequencing, where mRNA and small RNA sequencing libraries were generated from the same total RNA samples in parallel. mRNA libraries were prepared by enrichment with oligo(dT) beads and sequenced on an Illumina

NovaSeq 6000 generating 150 bp paired-end libraries. Small RNA seq libraries were generated by 3' adapter ligation, 5' adapter ligation, reverse transcription, PCR amplification, and gel purification and size selection. Small RNA samples were sequenced on an Illumina Novaseq 6000 generating 50 nucleotide single-end read libraries. Raw sequencing data has been deposited to SRA under PRJNA854614.

mRNA-seq data pre-processing and genomic alignment

FASTQ reads from mRNA libraries were first hard-trimmed using fastx_trimmer (fastx_toolkit 0.0.13) (Gordon A., 2010), to remove 5' adapter fragments and low quality bases at the 3' end of the reads using parameters "-f 16", "-l 100", and "-Q33". Next, Illumina adapters were removed using TrimGalore 0.6.7 (cutadapt 3.3) (Felix Krueger, 2021). To maximize our capture of relevant reads, we used the most contiguous genome reference currently available for the African turquoise killifish, Genbank accession GCA_014300015.1, described in Williamsen *et al.,* 2020 (Willemsen *et al.*, 2020), as well as its corresponding gene annotation file. Since analysis of repetitive sequences was desired, we performed soft-masking with Repeatmasker 4.1.2-p1 (Smit, 2013-2015) and a turquoise killifish specific consensus TE library downloaded from FishTEDB (downloaded: February 5, 2021) (Shao et al., 2018). A TE-specific GTF file for downstream analysis was generated using a custom R script for compatibility with the TETranscripts counting program (Jin et al., 2015). RNA-seq reads were aligned to the soft-masked turquoise killifish genome using STAR 2.7.0e, allowing 200 multimappers to accommodate TE sequence alignment (Dobin et al., 2013; Jin *et al.*, 2015). Gene and TE counts were generated using TETranscripts 2.2.1 with default settings using gene annotations from GenBank and the RepeatMasker derived custom TE-specific GTF file.

Differential gene and TE expression analysis

The TETranscripts count matrices for genes and TEs were analyzed together in R 4.1.2 using DESeq2 v1.34.0 (Love *et al.*, 2014). For global analyses of transcriptional aging patterns across testes and ovaries, all samples were analyzed together, using sex and age as model covariates (**Figs. 1D-F**). Principal component analysis (PCA) plots were generated from the normalized gene and TE were generated for each biological replicate. To identify differentially expressed transcripts and their patterns with aging in ovaries and testes, we used likelihood ratio testing [LRT] separately for each sex with each age as its own group. Significant genes were defined as those with an adjusted p-value of < 1E-6 with the DESeq2 LRT test. Genes and TEs were then analyzed separately. Once significantly differentially expressed genes and TEs were identified, clusters of differentially expressed genes and TEs were unbiasedly identified using the 'degPatterns' function from the 'DEGreport' v1.30.3 package (Pantano, 2022).

Fractional TE analysis

To compare fractional TE expression in killifish gonads, the TEtranscripts count matrices used for differential gene and TE expression analysis were imported into R. For each biological replicate, assigned counts were classified as genic or TE-derived and the fractional TE representation for each replicate library was calculated as TE read counts divided by total read counts. Fractional counts were grouped by age and sex and tested for significance by the non-parametric Wilcoxon rank sum test between groups within each sex.

Functional enrichment analysis

Data was prepared for functional enrichment analysis by running blastp (ncbi-blast v2.13.0) with African turquoise killifish protein sequences from the (Willemsen, 2020) GCA_014300015.1 genome version, against Ensembl release 104 human protein sequences. For each query killifish sequence, only top hits with E-value < 1e-3 were retained, and these human homologs were used for functional enrichment analyses. Gene ontology (GO) enrichment analysis was performed using 'GOstats' 2.60.0 with GO terms downloaded using 'biomaRt' 2.50.3 (Durinck et al., 2009) corresponding to Ensembl release 104. GO analysis was performed using the "Biological Process", "Cellular Component", and "Molecular Function" categories with a significance threshold equal to a false discovery rate [FDR] < 5%. GO analysis was performed on each of the gene patterns identified in the LRT-based DGE analysis described above.

piRNA selection, annotation, and piRNA cluster analyses

FASTQ reads from small RNA libraries were trimmed of their adapters while keeping a minial length of at least 18 nucleotides using TrimGalore 0.6.7 (cutadapt 3.3) (Felix Krueger, 2021) with the commands "--length 18", "-a GTTCAGAGTTCTACAGTCCGACGATC", and "-a GTTCAGAGTTCTACAGTCCGACGATC". piRNAs were selected by size-selecting sequences between 24-35 nucleotides in length from the trimmed small RNA libraries (Gong *et al.*, 2018; Huang *et al.*, 2019). piRNA length distributions (**Fig. S5A**) were generated by combining piRNA length histogram data by sex and plotting the resultant length distribution in R. piRNA nucleotide distribution for each sex was computed by converting piRNA reads to fasta format files and concatenating by sex. Position weight matrices were generated from these fasta files in R using the package 'Biostrings' 2.58.0 (**Fig. 5B**). Sequence logos were generated from position weight matrices using the R package 'ggseqlogo' 0.1.

To identify piRNA clusters, we used the Protrac 2.42 software suite (Rosenkranz and Zischler, 2012). Briefly, piRNAs were collapsed to unique reads, while retaining count numbers using the functions TBr2_collapse.pl and TBr2_duster.pl. These reads were then mapped to

the soft-masked reference genome described previously using the function sRNAmapper.pl and clusters were identified by a preponderance of piRNA mapping within a particular window using the function proTRAC_2.4.3.pl. Clusters were identified for each biological replicate before being combined such that only unique piRNA clusters remained using the Protrac function merge.pl. To assess the TE composition of piRNA clusters relative to the genome, the intersectbed command (bedtools 2.27.1) was used to extract piRNA cluster fasta sequences from the genome (Quinlan and Hall, 2010). Then, Repeatmasker 4.1.2-p1 was run as above on the isolated piRNA cluster fasta sequences to obtain TE family information, which was then contrasted with the genome-wide data in R.

piRNA differential expression and Ping-Pong analysis

piRNAs were mapped to the soft-masked genome reference using bowtie 1.2.3 (Langmead et al., 2009) with three allowed mismatches since piRNAs are known to bind with imperfect basepairing (George et al., 2015; Juliano et al., 2014; Teefy *et al.*, 2020; Zhang et al., 2015) using the parameters "-v 3 -a --best --strata -S" before being converted to bam format files with samtools 1.10 (Danecek et al., 2021). piRNA counts were then assigned using 'featureCounts' from the Subread 2.0.2 package, using fractional count attribution for multimapping reads (Liao et al., 2014). For featureCounts based read counting, a custom GTF file consisting of genes, TEs, piRNA clusters, and rRNA repeats as features was used to account for piRNA mapping to all relevant features to minimize biases in piRNA counts. The resultant count matrix was imported into R, and rRNA-mapping reads were discarded prior to normalization. Then piRNA counts that mapped to genes, TEs, and piRNA clusters were normalized together using DEseq2. LRT-based clustering and DGE analysis was then performed for piRNA counts that mapped to TE sequences as described above.

To measure ping-pong biogenesis, we only considered piRNAs mapping to consensus TE sequences, since they constitute the most biologically relevant target of gonadal piRNAs. To analyze ping-pong biogenesis at a global level, we used the PPmeter 0.4 program (Jehn *et al.*, 2018). Briefly, PPmeter reports the rate of 10 bp overlaps between piRNA reads, a proxy for ping-pong biogenesis, by generating pseudo-replicates through boostrapping one million piRNA reads (100 bootstraps). Using this approach, piRNA libraries can be directly compared to each other by measuring the number of ping-pong events (*i.e.* 10 bp overlaps) per one million piRNA reads. The resultant metric, ping-pong rate per million bootstrapped reads (ppr-mbr) was calculated for each bootstrap in each piRNA library. Bootstrap values were combined per biological replicate and the median value was taken. Median ppr-mbr values were then grouped by age and sex and tested for statistical difference by age group within each sex by the non-parametric Wilcoxon rank sum test.

For TE-specific level ping-pong measurement, we used custom scripts that calculated Z_{10} scores for each consensus TE sequence. Z_{10} scores, as defined in (Han *et al.*, 2015; Vandewege *et al.*, 2022) is the difference of 10 bp overlap occurrences and the mean of all other overlap occurrences within a 20 bp window divided by the standard deviation of all other overlap occurrences. This is shown in the following equation:

$$Z_{10} = \frac{(10\ bp\ overlaps) - (\mu_{1:9,11:20\ bp}\ overlaps)}{\sigma_{1:9,11:20\ bp}\ overlaps}$$

To generate Z_{10} scores, the distances between piRNA 5' ends that mapped to opposite strands of consensus TE sequences were tabulated into a histogram using a custom bash script. The resultant histograms were imported into R and processed in a custom script that reported the Z_{10} score for each consensus TE sequence. For some TE sequences, coverage was incomplete such that we could not derive Z_{10}-score information; these sequences were discarded from consideration. To measure the changes in Z_{10} scores with age, TE Z_{10} scores were separated by sex and grouped by age. Group-level Z_{10} scores were tested for significant differences by 1-way ANOVA in R, and only TEs with an adjusted p-value <0.05 were considered significantly regulated with aging in either gonad type. Significant TEs were then classified into clusters using the 'degPatterns' function from 'DEGreport' 1.30.3 package as described previously. For biological group-level analysis of Z_{10} scores, median Z_{10} values over all detected TE sequences were taken for each biological replicate and plotted as a function of age and sex. Difference in Z_{10} scores per group were tested between age groups within sexes by a non-parametric Wilcoxon rank sum test.

Data and code availability

All scripts used in this study are available on the Benayoun laboratory Github (https://github.com/BenayounLaboratory/Killifish_reproductive_aging_resource). All R scripts were run using R version 4.1.2. mRNA and piRNA FASTQ reads were deposited to the NCBI Sequence Read Archive under BioProject accession PRJNA854614.

Acknowledgments

Some panels were made with BioRender.com. We thank Suchi Patel of the USC Genome Core for running RNA bioanalyzer assays. We thank Jomille Jerez, Isabel Ollerton, Rajyk Bhala and Katelyn Hsu for assistance with killifish husbandry. We thank Dr. Carolyn Phillips, Justin Gilmore, Juan Bravo, Casandra McGill, Dr. Minhoo Kim, and Rajyk Bhala for insights and feedback on our manuscript. This work was supported by an NIA T32 AG052374 Postdoctoral Training Grant fellowship to B.B.T, NIA R21 AG063739, NIGMS R35 GM142395, a pilot grant from the NAVIGAGE Foundation, and a Hanson-Thorell Family award to B.A.B.

The authors acknowledge the Center for Advanced Research Computing (CARC) at the University of Southern California for providing computing resources that have contributed to the research results reported within this publication (https://carc.usc.edu).

Author contributions

B.B.T. and B.A.B. designed the study. B.B.T. and A.A. performed fish husbandry. A.A. dissected killifish gonadal tissues. B.B.T. performed RNA extraction of samples and computational analyses, with assistance from A.X., P.P.S. and B.A.B. B.B.T. and B.A.B. wrote the manuscript with input from all authors. All authors edited and commented on the manuscript.

References

Akagi, K., Li, J., and Symer, D.E. (2013). How do mammalian transposons induce genetic variation? A conceptual framework: the age, structure, allele frequency, and genome context of transposable elements may define their wide-ranging biological impacts. Bioessays *35*, 397-407. 10.1002/bies.201200133.

Alberts, S.C., Altmann, J., Brockman, D.K., Cords, M., Fedigan, L.M., Pusey, A., Stoinski, T.S., Strier, K.B., Morris, W.F., and Bronikowski, A.M. (2013). Reproductive aging patterns in primates reveal that humans are distinct. Proc Natl Acad Sci U S A *110*, 13440-13445. 10.1073/pnas.1311857110.

Bariah, I., Keidar-Friedman, D., and Kashkush, K. (2020). Where the Wild Things Are: Transposable Elements as Drivers of Structural and Functional Variations in the Wheat Genome. Front Plant Sci *11*, 585515. 10.3389/fpls.2020.585515.

Baumgart, M., Priebe, S., Groth, M., Hartmann, N., Menzel, U., Pandolfini, L., Koch, P., Felder, M., Ristow, M., Englert, C., et al. (2016). Longitudinal RNA-Seq Analysis of Vertebrate Aging Identifies Mitochondrial Complex I as a Small-Molecule-Sensitive Modifier of Lifespan. Cell Syst *2*, 122-132. 10.1016/j.cels.2016.01.014.

Belyayev, A. (2014). Bursts of transposable elements as an evolutionary driving force. J Evol Biol *27*, 2573-2584. 10.1111/jeb.12513.

Ben Maamar, M., Nilsson, E.E., and Skinner, M.K. (2021). Epigenetic transgenerational inheritance, gametogenesis and germline developmentdagger. Biol Reprod *105*, 570-592. 10.1093/biolre/ioab085.

Benayoun, B.A., Pollina, E.A., Singh, P.P., Mahmoudi, S., Harel, I., Casey, K.M., Dulken, B.W., Kundaje, A., and Brunet, A. (2019). Remodeling of epigenome and transcriptome landscapes with aging in mice reveals widespread induction of inflammatory responses. Genome Res *29*, 697-709. 10.1101/gr.240093.118.

Bertoldo, M.J., Listijono, D.R., Ho, W.J., Riepsamen, A.H., Goss, D.M., Richani, D., Jin, X.L., Mahbub, S., Campbell, J.M., Habibalahi, A., et al. (2020). NAD(+) Repletion Rescues Female Fertility during Reproductive Aging. Cell Rep *30*, 1670-1681 e1677. 10.1016/j.celrep.2020.01.058.

Bravo, J.I., Nozownik, S., Danthi, P.S., and Benayoun, B.A. (2020). Transposable elements, circular RNAs and mitochondrial transcription in age-related genomic regulation. Development *147*. 10.1242/dev.175786.

Catlin, N.S., and Josephs, E.B. (2022). The important contribution of transposable elements to phenotypic variation and evolution. Curr Opin Plant Biol *65*, 102140. 10.1016/j.pbi.2021.102140.

Chen, H., Zheng, X., Xiao, D., and Zheng, Y. (2016). Age-associated de-repression of retrotransposons in the Drosophila fat body, its potential cause and consequence. Aging Cell *15*, 542-552. 10.1111/acel.12465.

Chen, J., Lu, L., Robb, S.M.C., Collin, M., Okumoto, Y., Stajich, J.E., and Wessler, S.R. (2020). Genomic diversity generated by a transposable element burst in a rice recombinant inbred population. Proc Natl Acad Sci U S A *117*, 26288-26297. 10.1073/pnas.2015736117.

Chen, P., Kotov, A.A., Godneeva, B.K., Bazylev, S.S., Olenina, L.V., and Aravin, A.A. (2021). piRNA-mediated gene regulation and adaptation to sex-specific transposon expression in D. melanogaster male germline. Genes Dev *35*, 914-935. 10.1101/gad.345041.120.

Core, H.C.B. (2021). DGE analysis using LRT in DESeq2. https://hbctraining.github.io/DGE_workshop_salmon/lessons/08_DGE_LRT.html.

Cui, R., Medeiros, T., Willemsen, D., Iasi, L.N.M., Collier, G.E., Graef, M., Reichard, M., and Valenzano, D.R. (2020). Relaxed Selection Limits Lifespan by Increasing Mutation Load. Cell *180*, 1272-1279. 10.1016/j.cell.2020.02.038.

Czech, B., and Hannon, G.J. (2016). One Loop to Rule Them All: The Ping-Pong Cycle and piRNA-Guided Silencing. Trends Biochem Sci *41*, 324-337. 10.1016/j.tibs.2015.12.008.

Dabrowski, R., Ripa, R., Latza, C., Annibal, A., and Antebi, A. (2020). Optimization of mass spectrometry settings for steroidomic analysis in young and old killifish. Anal Bioanal Chem *412*, 4089-4099. 10.1007/s00216-020-02640-6.

Danecek, P., Bonfield, J.K., Liddle, J., Marshall, J., Ohan, V., Pollard, M.O., Whitwham, A., Keane, T., McCarthy, S.A., Davies, R.M., and Li, H. (2021). Twelve years of SAMtools and BCFtools. Gigascience *10*. 10.1093/gigascience/giab008.

De Cecco, M., Criscione, S.W., Peterson, A.L., Neretti, N., Sedivy, J.M., and Kreiling, J.A. (2013). Transposable elements become active and mobile in the genomes of aging mammalian somatic tissues. Aging (Albany NY) *5*, 867-883. 10.18632/aging.100621.

Dobin, A., Davis, C.A., Schlesinger, F., Drenkow, J., Zaleski, C., Jha, S., Batut, P., Chaisson, M., and Gingeras, T.R. (2013). STAR: ultrafast universal RNA-seq aligner. Bioinformatics *29*, 15-21. 10.1093/bioinformatics/bts635.

Dodzian, J., Kean, S., Seidel, J., and Valenzano, D.R. (2018). A Protocol for Laboratory Housing of Turquoise Killifish (Nothobranchius furzeri). J Vis Exp. 10.3791/57073.

Durinck, S., Spellman, P.T., Birney, E., and Huber, W. (2009). Mapping identifiers for the integration of genomic datasets with the R/Bioconductor package biomaRt. Nat Protoc *4*, 1184-1191. 10.1038/nprot.2009.97.

Erwin, A.A., and Blumenstiel, J.P. (2019). Aging in the Drosophila ovary: contrasting changes in the expression of the piRNA machinery and mitochondria but no global release of transposable elements. BMC Genomics *20*, 305. 10.1186/s12864-019-5668-3.

Falcon, S., and Gentleman, R. (2007). Using GOstats to test gene lists for GO term association. Bioinformatics *23*, 257-258. 10.1093/bioinformatics/btl567.

Felix Krueger, F.J., Phil Ewels, Ebrahim Afyounian, & Benjamin Schuster-Boeckler (2021). FelixKrueger/TrimGalore: v0.6.7 - DOI via Zenodo (0.6.7). Zenodo. https://doi.org/10.5281/zenodo.5127899. Accessed August 20, 2021.

Finch, C.E. (2014). The menopause and aging, a comparative perspective. J Steroid Biochem Mol Biol *142*, 132-141. 10.1016/j.jsbmb.2013.03.010.

George, P., Jensen, S., Pogorelcnik, R., Lee, J., Xing, Y., Brasset, E., Vaury, C., and Sharakhov, I.V. (2015). Increased production of piRNAs from euchromatic clusters and genes in Anopheles gambiae compared with Drosophila melanogaster. Epigenetics Chromatin *8*, 50. 10.1186/s13072-015-0041-5.

Gong, J., Zhang, Q., Wang, Q., Ma, Y., Du, J., Zhang, Y., and Zhao, X. (2018). Identification and verification of potential piRNAs from domesticated yak testis. Reproduction *155*, 117-127. 10.1530/REP-17-0592.

Gonzalez, J., Karasov, T.L., Messer, P.W., and Petrov, D.A. (2010). Genome-wide patterns of adaptation to temperate environments associated with transposable elements in Drosophila. PLoS Genet *6*, e1000905. 10.1371/journal.pgen.1000905.

Gordon A., H.G. (2010). FASTX-Toolkit. Unpublished.

Gunes, S., Hekim, G.N., Arslan, M.A., and Asci, R. (2016). Effects of aging on the male reproductive system. J Assist Reprod Genet *33*, 441-454. 10.1007/s10815-016-0663-y.

Han, B.W., Wang, W., Li, C., Weng, Z., and Zamore, P.D. (2015). Noncoding RNA. piRNA-guided transposon cleavage initiates Zucchini-dependent, phased piRNA production. Science *348*, 817-821. 10.1126/science.aaa1264.

Harel, I., Valenzano, D.R., and Brunet, A. (2016). Efficient genome engineering approaches for the short-lived African turquoise killifish. Nat Protoc *11*, 2010-2028. 10.1038/nprot.2016.103.

Hu, C.K., and Brunet, A. (2018). The African turquoise killifish: A research organism to study vertebrate aging and diapause. Aging Cell *17*, e12757. 10.1111/acel.12757.

Huang, S., Ichikawa, Y., Igarashi, Y., Yoshitake, K., Kinoshita, S., Omori, F., Maeyama, K., Nagai, K., Watabe, S., and Asakawa, S. (2019). Piwi-interacting RNA (piRNA) expression patterns in pearl oyster (Pinctada fucata) somatic tissues. Sci Rep *9*, 247. 10.1038/s41598-018-36726-0.

Jehn, J., Gebert, D., Pipilescu, F., Stern, S., Kiefer, J.S.T., Hewel, C., and Rosenkranz, D. (2018). PIWI genes and piRNAs are ubiquitously expressed in mollusks and show patterns of lineage-specific adaptation. Commun Biol *1*, 137. 10.1038/s42003-018-0141-4.

Jin, Y., Tam, O.H., Paniagua, E., and Hammell, M. (2015). TEtranscripts: a package for including transposable elements in differential expression analysis of RNA-seq datasets. Bioinformatics *31*, 3593-3599. 10.1093/bioinformatics/btv422.

Jones, O.R., Scheuerlein, A., Salguero-Gomez, R., Camarda, C.G., Schaible, R., Casper, B.B., Dahlgren, J.P., Ehrlen, J., Garcia, M.B., Menges, E.S., et al. (2014). Diversity of ageing across the tree of life. Nature *505*, 169-173. 10.1038/nature12789.

Juliano, C.E., Reich, A., Liu, N., Gotzfried, J., Zhong, M., Uman, S., Reenan, R.A., Wessel, G.M., Steele, R.E., and Lin, H. (2014). PIWI proteins and PIWI-interacting RNAs function in Hydra somatic stem cells. Proc Natl Acad Sci U S A *111*, 337-342. 10.1073/pnas.1320965111.

Kenny, L.C., Lavender, T., McNamee, R., O'Neill, S.M., Mills, T., and Khashan, A.S. (2013). Advanced maternal age and adverse pregnancy outcome: evidence from a large contemporary cohort. PLoS One *8*, e56583. 10.1371/journal.pone.0056583.

Ketting, R.F. (2011). The many faces of RNAi. Dev Cell *20*, 148-161. 10.1016/j.devcel.2011.01.012.

Kim, Y., Nam, H.G., and Valenzano, D.R. (2016). The short-lived African turquoise killifish: an emerging experimental model for ageing. Dis Model Mech *9*, 115-129. 10.1242/dmm.023226.

Langmead, B., Trapnell, C., Pop, M., and Salzberg, S.L. (2009). Ultrafast and memory-efficient alignment of short DNA sequences to the human genome. Genome Biol *10*, R25. 10.1186/gb-2009-10-3-r25.

LaRocca, T.J., Cavalier, A.N., and Wahl, D. (2020). Repetitive elements as a transcriptomic marker of aging: Evidence in multiple datasets and models. Aging Cell *19*, e13167. 10.1111/acel.13167.

Liao, Y., Smyth, G.K., and Shi, W. (2014). featureCounts: an efficient general purpose program for assigning sequence reads to genomic features. Bioinformatics *30*, 923-930. 10.1093/bioinformatics/btt656.

Lin, K.Y., Wang, W.D., Lin, C.H., Rastegari, E., Su, Y.H., Chang, Y.T., Liao, Y.F., Chang, Y.C., Pi, H., Yu, B.Y., et al. (2020). Piwi reduction in the aged niche eliminates germline stem cells via Toll-GSK3 signaling. Nat Commun *11*, 3147. 10.1038/s41467-020-16858-6.

Liu, Y., Kassack, M.E., McFaul, M.E., Christensen, L.N., Siebert, S., Wyatt, S.R., Kamei, C.N., Horst, S., Arroyo, N., Drummond, I.A., et al. (2022). Single-cell transcriptome reveals insights into the development and function of the zebrafish ovary. Elife *11*. 10.7554/eLife.76014.

Love, M.I., Huber, W., and Anders, S. (2014). Moderated estimation of fold change and dispersion for RNA-seq data with DESeq2. Genome Biol *15*, 550. 10.1186/s13059-014-0550-8.

Malki, S., van der Heijden, G.W., O'Donnell, K.A., Martin, S.L., and Bortvin, A. (2014). A role for retrotransposon LINE-1 in fetal oocyte attrition in mice. Dev Cell *29*, 521-533. 10.1016/j.devcel.2014.04.027.

Mani, S.R., and Juliano, C.E. (2013). Untangling the web: the diverse functions of the PIWI/piRNA pathway. Mol Reprod Dev *80*, 632-664. 10.1002/mrd.22195.

McClintock, B. (1984). The significance of responses of the genome to challenge. Science *226*, 792-801. 10.1126/science.15739260.

Mira, A. (1998). Why is meiosis arrested? J Theor Biol *194*, 275-287. 10.1006/jtbi.1998.0761.

Naumann, B., and Englert, C. (2018). Dispersion/reaggregation in early development of annual killifishes: Phylogenetic distribution and evolutionary significance of a unique feature. Dev Biol *442*, 69-79. 10.1016/j.ydbio.2018.07.015.

Pantano, L. (2022). DEGreport: Report of DEG analysis. R package version 1.30.3. http://lpantano.github.io/DEGreport/.

Perheentupa, A., and Huhtaniemi, I. (2009). Aging of the human ovary and testis. Mol Cell Endocrinol *299*, 2-13. 10.1016/j.mce.2008.11.004.

Quinlan, A.R., and Hall, I.M. (2010). BEDTools: a flexible suite of utilities for comparing genomic features. Bioinformatics *26*, 841-842. 10.1093/bioinformatics/btq033.

Reichwald, K., Petzold, A., Koch, P., Downie, B.R., Hartmann, N., Pietsch, S., Baumgart, M., Chalopin, D., Felder, M., Bens, M., et al. (2015). Insights into Sex Chromosome Evolution and Aging from the Genome of a Short-Lived Fish. Cell *163*, 1527-1538. 10.1016/j.cell.2015.10.071.

Roovers, E.F., Rosenkranz, D., Mahdipour, M., Han, C.T., He, N., Chuva de Sousa Lopes, S.M., van der Westerlaken, L.A., Zischler, H., Butter, F., Roelen, B.A., and Ketting, R.F. (2015). Piwi proteins and piRNAs in mammalian oocytes and early embryos. Cell Rep *10*, 2069-2082. 10.1016/j.celrep.2015.02.062.

Rosenberg, A.M., Rausser, S., Ren, J., Mosharov, E.V., Sturm, G., Ogden, R.T., Patel, P., Kumar Soni, R., Lacefield, C., Tobin, D.J., et al. (2021). Quantitative mapping of human hair greying and reversal in relation to life stress. Elife *10*. 10.7554/eLife.67437.

Rosenkranz, D., and Zischler, H. (2012). proTRAC--a software for probabilistic piRNA cluster detection, visualization and analysis. BMC Bioinformatics *13*, 5. 10.1186/1471-2105-13-5.

Sahu, S., Dattani, A., and Aboobaker, A.A. (2017). Secrets from immortal worms: What can we learn about biological ageing from the planarian model system? Semin Cell Dev Biol *70*, 108-121. 10.1016/j.semcdb.2017.08.028.

Sargent, K.M., McFee, R.M., Spuri Gomes, R., and Cupp, A.S. (2015). Vascular endothelial growth factor A: just one of multiple mechanisms for sex-specific vascular development within the testis? J Endocrinol *227*, R31-50. 10.1530/JOE-15-0342.

Schaible, R., Scheuerlein, A., Danko, M.J., Gampe, J., Martinez, D.E., and Vaupel, J.W. (2015). Constant mortality and fertility over age in Hydra. Proc Natl Acad Sci U S A *112*, 15701-15706. 10.1073/pnas.1521002112.

Shao, F., Wang, J., Xu, H., and Peng, Z. (2018). FishTEDB: a collective database of transposable elements identified in the complete genomes of fish. Database (Oxford) *2018*. 10.1093/database/bax106.

Sharov, A.A., Falco, G., Piao, Y., Poosala, S., Becker, K.G., Zonderman, A.B., Longo, D.L., Schlessinger, D., and Ko, M. (2008). Effects of aging and calorie restriction on the global gene expression profiles of mouse testis and ovary. BMC Biol *6*, 24. 10.1186/1741-7007-6-24.

Simon, M., Van Meter, M., Ablaeva, J., Ke, Z., Gonzalez, R.S., Taguchi, T., De Cecco, M., Leonova, K.I., Kogan, V., Helfand, S.L., et al. (2019). LINE1 Derepression in Aged Wild-Type and SIRT6-Deficient Mice Drives Inflammation. Cell Metab *29*, 871-885 e875. 10.1016/j.cmet.2019.02.014.

Smit, A., Hubley, R & Green, P. (2013-2015). RepeatMasker Open-4.0. <http://www.repeatmasker.org>. Accessed August 20, 2021.

Sousa-Victor, P., Ayyaz, A., Hayashi, R., Qi, Y., Madden, D.T., Lunyak, V.V., and Jasper, H. (2017). Piwi Is Required to Limit Exhaustion of Aging Somatic Stem Cells. Cell Rep *20*, 2527-2537. 10.1016/j.celrep.2017.08.059.

Teefy, B.B., Siebert, S., Cazet, J.F., Lin, H., and Juliano, C.E. (2020). PIWI-piRNA pathway-mediated transposable element repression in Hydra somatic stem cells. RNA *26*, 550-563. 10.1261/rna.072835.119.

Terzibasi Tozzini, E., and Cellerino, A. (2020). Nothobranchius annual killifishes. Evodevo *11*, 25. 10.1186/s13227-020-00170-x.

Thomson, T., and Lin, H. (2009). The biogenesis and function of PIWI proteins and piRNAs: progress and prospect. Annu Rev Cell Dev Biol *25*, 355-376. 10.1146/annurev.cellbio.24.110707.175327.

Valenzano, D.R., Benayoun, B.A., Singh, P.P., Zhang, E., Etter, P.D., Hu, C.K., Clement-Ziza, M., Willemsen, D., Cui, R., Harel, I., et al. (2015). The African Turquoise Killifish Genome Provides Insights into Evolution and Genetic Architecture of Lifespan. Cell *163*, 1539-1554. 10.1016/j.cell.2015.11.008.

Valenzano, D.R., Sharp, S., and Brunet, A. (2011). Transposon-Mediated Transgenesis in the Short-Lived African Killifish Nothobranchius furzeri, a Vertebrate Model for Aging. G3 (Bethesda) *1*, 531-538. 10.1534/g3.111.001271.

Vandewege, M.W., Patt, R.N., 2nd, Merriman, D.K., Ray, D.A., and Hoffmann, F.G. (2022). The PIWI/piRNA response is relaxed in a rodent that lacks mobilizing transposable elements. RNA *28*, 609-621. 10.1261/rna.078862.121.

Vrtilek, M., Zak, J., Psenicka, M., and Reichard, M. (2018). Extremely rapid maturation of a wild African annual fish. Curr Biol *28*, R822-R824. 10.1016/j.cub.2018.06.031.

Wang, W., Han, B.W., Tipping, C., Ge, D.T., Zhang, Z., Weng, Z., and Zamore, P.D. (2015). Slicing and Binding by Ago3 or Aub Trigger Piwi-Bound piRNA Production by Distinct Mechanisms. Mol Cell *59*, 819-830. 10.1016/j.molcel.2015.08.007.

Watanabe, T., Totoki, Y., Toyoda, A., Kaneda, M., Kuramochi-Miyagawa, S., Obata, Y., Chiba, H., Kohara, Y., Kono, T., Nakano, T., et al. (2008). Endogenous siRNAs from naturally formed dsRNAs regulate transcripts in mouse oocytes. Nature *453*, 539-543. 10.1038/nature06908.

Willemsen, D., Cui, R., Reichard, M., and Valenzano, D.R. (2020). Intra-species differences in population size shape life history and genome evolution. Elife *9*. 10.7554/eLife.55794.

Yamashiro, H., and Siomi, M.C. (2018). PIWI-Interacting RNA in Drosophila: Biogenesis, Transposon Regulation, and Beyond. Chem Rev *118*, 4404-4421. 10.1021/acs.chemrev.7b00393.

Yang, N., Srivastav, S.P., Rahman, R., Ma, Q., Dayama, G., Li, S., Chinen, M., Lei, E.P., Rosbash, M., and Lau, N.C. (2022). Transposable element landscapes in aging Drosophila. PLoS Genet *18*, e1010024. 10.1371/journal.pgen.1010024.

Zak, J., and Reichard, M. (2021). Reproductive senescence in a short-lived fish. J Anim Ecol *90*, 492-502. 10.1111/1365-2656.13382.

Zhang, P., Kang, J.Y., Gou, L.T., Wang, J., Xue, Y., Skogerboe, G., Dai, P., Huang, D.W., Chen, R., Fu, X.D., et al. (2015). MIWI and piRNA-mediated cleavage of messenger RNAs in mouse testes. Cell Res *25*, 193-207. 10.1038/cr.2015.4.

Legends to Figures

Figure 1. A study of gonadal aging in the naturally short-lived African turquoise killifish

(A) Experimental scheme for killifish gonad sequencing. Killifish gonads (N = 5) were dissected and total RNA was extracted. Only high quality RNA samples (RIN>7) were included for further processing (see **Fig. S1A**). Small RNA and mRNA RNA-seq libraries were derived from each total RNA sample and sequenced for downstream analyses. **(B)** Lifespan curve for female and male GRZ strain killifish at the USC Benayoun lab facility. GRZ females lived significantly longer than males (p = 0.002; log Rank test). Median lifespan of females: 26.55 weeks, males: 19.4 weeks. Vertical dotted lines: ages sampled in this study (5, 10, 15 weeks), chosen to represent aging before substantially decreased population survival. **(C-E)** Principal component analyses [PCAs] for **(C)** mRNA gene expression **(D)** TE expression and **(E)** TE-mapping piRNA abundance (see methods).

Figure 2. Differential gene expression analysis and GO Biological Process functional enrichment analysis with ovarian aging.

(A) Scheme used for differential gene expression [DGE] analysis used in this study. DGE was performed with DESeq2's likelihood ratio testing [LRT], which revealed 4 approximate groups of differentially expressed genes corresponding to expression (a) Down at Middle-Age, (b) Up at Middle-Age, (c) Down with Age and (d) Up with Age. **(B)** Heatmaps of gene expression for genes significantly regulated with age in aging killifish ovaries by DEseq2 LRT (FDR < 1e-6). Most differentially expressed genes transiently changed at middle-age. **(C)** Functional enrichment analysis for each gene cluster in **Fig. 2B**, showing the top 10 most significant GO "Biological Process" terms by 'GOstats' (FDR < 5%; see **Supplementary Table S3A** for complete list of enriched terms). The most significant term downregulated in middle-aged ovaries is "piRNA metabolic process" (bolded). FDR: False discovery rate. Enrichment: fold enrichment over background.

Figure 3. Differential gene expression and GO Biological Process functional enrichment analysis with testicular aging.

(A) Heatmaps of gene expression for genes significantly regulated with age in aging killifish testes by DEseq2 LRT (FDR < 1e-6). Groups correspond to those defined in **Fig. 2A**. Like ovaries, most differential gene expression in killifish testes occurs transiently at middle-age. **(B)** Functional enrichment analysis for each gene cluster shown in **Fig. 3A** showing the top 10 most significant GO "Biological Process" terms by 'GOstats' (FDR < 5%; see **Supplementary Table S3D** for complete list of enriched terms). Genes that are upregulated in middle-age testis are enriched for terms related to spermatogenesis. Note that cluster (d)

(genes up with age) had too few genes to generate meaningful enrichment results. FDR: False discovery rate. Enrichment: fold enrichment over background.

Figure 4. TE expression dynamics in the aging turquoise killifish gonad.

(A) Experimental scheme for TE transcriptional analysis in aging gonads. Fractional TE counts were computed by counting the number of TE counts over total assigned mRNA-seq counts (genes and TEs). TE DGE was conducted in the same manner as the genic DGE analysis (see methods), and were labelled with the cluster nomenclature from **Fig. 2A**. **(B)** Proportion of assigned reads allocated to TEs from each mRNA-seq library for ovaries and testes. Significance in non-parametric Wilcoxon Rank Sum test. Note that old ovaries have significantly fewer proportional TE counts relative to middle-aged ovaries, and that testes seem to show a marginal increase in TE transcription with aging. **(C)** Heatmaps of mRNA expression for TEs significantly regulated with age in aging killifish ovaries by DEseq2 LRT (FDR < 1e-6). Each TE family is color-coded by row, revealing no obvious bias or enrichment for a specific TE type. **(D)** Heatmaps of mRNA expression for TEs significantly regulated with age in aging killifish testes by DEseq2 LRT (FDR < 1e-6). The only age differentially regulated TEs in the turquoise killifish testis are transiently upregulated at middle-age.

Figure 5. PIWI pathway activity and piRNA abundance characterization in aging turquoise killifish gonads.

(A) Heatmaps of normalized gene expression from ovaries and testes with aging in the GO "piRNA metabolic pathway" term. Killifish gene names and their best human homologs are indicated for each row. Rows were normalized by the median expression level in the cognate young gonad, so as to facilitate visualization of age-related changes. Genes involved in this pathway tend to be significantly downregulated in middle-aged ovaries (see **Fig. 2C**). **(B)** Sequence logo plots of piRNA nucleotide composition from ovaries and testes, using data for each gonad type pooled across ages and replicates. As expected for piRNAs, killifish piRNAs show a strong position 1-U bias. There is also a slight bias for Adenine at position 10, consistent with active ping-pong biogenesis in killifish gonads. **(C)** Stacked barplots depicting the TE family composition of piRNA clusters and the killifish genome, as a percentage of identified elements. The piRNA cluster TE composition is broadly reflective of the TE composition of the genome. **(D)** Heatmaps of TE-targeted piRNA abundance for TEs significantly regulated with age in aging killifish ovaries by DEseq2 LRT (FDR < 1e-6). TE family is color-coded for each row. In ovaries, most differentially piRNA-targeted TEs show a decrease of piRNA counts at middle-age. **(E)** Heatmaps of TE-targeted piRNA abundance for TEs significantly regulated with age in aging killifish testes by DEseq2 LRT (FDR < 1e-6). **(F)** Venn diagram of the overlap between TE_mapping piRNAs significantly upregulated in

middle-age ovaries (see **Fig. 5D**; pattern a) and TEs that are significantly downregulated in middle-age ovaries (see **Fig. 4C**; pattern b). Significance for the overlap being larger than expected by chance was calculated using Fisher's exact test, compared to TEs detected in both analyses. A pie chart of the composition of "consistent" TEs is also reported.

Figure 6. Analysis of ping-pong biogenesis in aging turquoise killifish gonads.
(A) Explanatory diagram of ping-pong biogenesis. PIWI1 (the PIWI protein loaded with 'primary' piRNAs complementary to TEs) binds to and cleaves a TE mRNA species. The cleaved TE mRNA is loaded into PIWI2 (the PIWI protein loaded with cleaved TE fragments, or 'TE-derived secondary' piRNAs). PIWI proteins always cleave their targets 10 basepairs from the 5' end of the piRNA. This mechanism, known as ping-pong biogenesis, will generate a preponderance of complementary piRNAs with a 10 basepair overlap, the detection of which is the basis of the assays shown in **Fig. 6B-F**. **(B)** Boxplot showing the median frequency of 10 basepair overlaps for 1 million piRNA reads over 100 bootstraps per biological sample (ppr-mbr: Ping-Pong Reads per Million Bootstrapped Reads,) as generated by PPmeter. Age groups within each sex were compared using the non-parametric Wilcoxon rank sum test. **(C)** Boxplot showing median Z_{10} scores over consensus TEs for each biological sample. Z_{10} scores are an alternative measure of ping-pong. Non-parametric Wilcoxon Rank Sum tests were used to test for significant differences between age groups. **(D)** Schematic for analysis of differential Z_{10} score patterns with gonadal aging. Z_{10} scores were generated for each consensus TE sequence in FishTEDB in each biological sample. An ANOVA test was run to detect any significant differences in Z_{10} score between age groups within each sex (FDR < 5%). Significant TEs were assigned to groups based on expression dynamics that align to the broad groups defined in **Fig. 2A**, with the detection of 2 new subgroups showing minimal expression at middle-age (a_1 and a_2), with highest Z_{10} scores in the young samples and old samples, respectively. **(E)** Heatmaps of differential Z_{10} scores with age in aging killifish ovaries by ANOVA (FDR < 5%). **(F)** Heatmaps of differential Z_{10} scores with age in aging killifish testes by ANOVA (FDR < 5%). A roughly equivalent amount of consensus TE sequences show linear up- and downregulation with age. The cognate TE family is color-coded by row, and does not reveal any specific bias.

Supplementary Material

Legends to Supplementary Figures:

Figure S1. Global Characterization of aging turquoise killifish gonadal Dataset.

(A) Description of datasets generated in this study. A total of 26 RNA-seq and 26 small RNA-seq datasets were generated from ovary and testes from ages 5, 10, and 15 weeks old. **(B-G)** PCA plots of (B) ovarian gene expression, (C) ovarian TE expression, (D) ovarian TE-targeted piRNA abundance, (E) testicular gene expression, (F) testicular TE expression, (G) testicular TE-targeted piRNA abundance.

Figure S2. Differential gene expression analysis and GO 'cellular component' enrichment analysis in aging turquoise killifish ovaries.

(A) Boxplots of differentially expressed gene expression groups in ovaries by DEseq2 LRT (FDR < 1e-6). Each dot represents the expression level of a significantly differentially expressed gene in each group normalized by Z-score for ease of group-to-group comparison. **(B)** Top 10 GO "Cellular Component" terms enriched in each associated cluster according to 'GOstats' (FDR < 5%; see **Supplementary Table S3B** for the complete list of enriched terms). Terms down at middle-age related to the PIWI pathway include "pi-body" and "P granule" terms. Patterns are labelled according to **Fig. 2A**. FDR: False discovery rate. Enrichment: fold enrichment over background.

Figure S3. Differential gene expression analysis and GO 'cellular component' enrichment analysis in aging turquoise killifish testes.

(A) Boxplots of differentially expressed gene expression groups in testes by DEseq2 LRT (FDR < 1e-6). Each dot represents the expression level of a significantly differentially expressed gene in each group normalized by Z-score for ease of group-to-group comparison. **(B)** Top 10 GO "Cellular Component" terms enriched in each associated cluster according to 'GOstats' (FDR < 5%; see **Supplementary Table S3E** for the complete list of enriched terms). Most terms enriched at middle-age are related to spermatogenesis. Patterns are labelled according to **Fig. 2A**. FDR: False discovery rate. Enrichment: fold enrichment over background.

Figure S4. TE expression dynamics in the gonads of aging turquoise killifish.

(A) Boxplots of significantly differentially expressed TE clusters in ovaries by DEseq2 LRT (FDR < 1e-6). **(B)** Boxplot of the differentially expressed TE clusters in testes by DEseq2 LRT (FDR < 1e-6). Each dot represents the expression level of a significantly differentially

expressed gene in each group normalized by Z-score for ease of group-to-group comparison. Patterns are labelled according to **Fig. 2A**.

Figure S5. piRNA characterization and regulation in aging turquoise killifish gonads.
(A) piRNA length distribution shown by sex, after computational filtering of small RNAs 24-35 bp. Both ovaries and testes have similar piRNA length profiles, with the majority of detected species at ~27bp. **(B)** Scatterplots of young, middle-aged, and old killifish ovaries normalized TE expression *vs.* piRNA counts assigned to the same cognate consensus TE sequence. There is a strong Spearman rank correlation Rho in all ovarian age groups (Rho = 0.66; significance of correlation test: $p < 2.2e-16$), indicating that piRNAs are produced sustainably throughout life in response to expressed TEs. **(C)** Scatterplots of young, middle-aged, and old killifish testes normalized TE expression *vs.* piRNA counts assigned to the same cognate consensus TE sequence . There is a slightly higher Spearman rank correlation in testes than ovaries (Rho = 0.74-0.75; significance of correlation test: $p < 2.2e-16$), likely reflecting a larger proportion of germ cells in testicular tissue. Rho: Spearman rank correlation value. **(D)** Boxplots of differentially piRNA-mapped groups of TEs in ovaries, by DEseq2 LRT (FDR < 1e-6), using the grouping arrangement defined in **Fig. 2A**. **(E)** Boxplots of differentially piRNA-mapped groups of TEs in testes by DEseq2 LRT (FDR < 1e-6).

Figure S6. Analysis of ping-pong biogenesis signatures in aging turquoise killifish gonads (continued).
(A) Median Z_i-scores in ovaries grouped by age measured for each position within a 20 basepair window as summarized for position 10 in **Fig. 6C**. The highest Z_i-score occurs at position 10 (corresponding to the Z_{10} value), indicating that ping-pong is occurring at all ages. **(B)** Median Z_i-scores in testes grouped by age measured for each position within a 20 basepair window. Like the ovarian samples, the highest Z_{10}-score occurs at position 10 indicating ping-pong activity. **(C)** Boxplots of differential Z_{10} scores of TEs grouped into patterns in ovaries (patterns defined in **Fig. 6D**). Each dot is the Z-normalized Z_{10} score per age group. **(D)** Boxplots of differential Z_{10} scores of TEs grouped into clusters in testes. Each dot is the Z-normalized Z_{10} score per age group.

Inventory of Supplemental Tables:

Supplementary Table S1: Lifespan and fecundity data from GRZ African turquoise killifish reported in this study.
(**A**) GRZ Lifespan Data (expressed in weeks) in the USC colony.

Supplementary Table S2: List of genes with differential expression significance with age by DESeq2 LRT (FDR < 1e-6), and expression of "piRNA metabolic pathway" GO term associated genes.
(**A**) Complete Genic Ovarian DESeq2 LRT Analysis with clusters. (**B**) Complete Genic Testicular DESeq2 LRT Analysis with clusters. (**C**) DEseq2 VST-Normalized $\log_2$(count) gene expression for "piRNA metabolic process" GO term (ovaries and testes). (**D**) Best BLAST hit with E-value < $1E^{-3}$ for turquoise killifish protein sequences aligning to Human Ensembl 104 protein sequences.

Supplementary Table S3: Enriched GO terms associated to genes with significant age-regulation in ovaries or testes (FDR < 5%).
(**A**) Ovarian Significantly enriched GO Biological Process Terms by clusters as defined in **Fig. 2A** (GOStats FDR <5%). (**B**) Ovarian Significantly enriched GO Cellular Component Terms by clusters as defined in **Fig. 2A** (GOStats FDR <5%). (**C**) Ovarian Significantly enriched GO Molecular Function Terms by clusters as defined in **Fig. 2A** (GOStats FDR <5%). (**D**) Testicular Significantly enriched GO Biological Process Terms by clusters as defined in **Fig. 2A** (GOStats FDR <5%). (**E**) Testicular Significantly enriched GO Cellular Component Terms by clusters as defined in **Fig. 2A** (GOStats FDR <5%). (**F**) Testicular Significantly enriched GO Molecular Function Terms by clusters as defined in **Fig. 2A** (GOStats FDR <5%).

Supplementary Table S4: List of TEs with differential expression significance with age by DESeq2 LRT (FDR < 1e-6).
(**A**) Complete TE Ovarian DESeq2 LRT Analysis with clusters as defined in **Fig. 2A**. (**B**) Complete TE Testicular DESeq2 LRT Analysis with clusters as defined in **Fig. 2A**.

Supplementary Table S5: List of piRNA targeted TE sequences with differential abundance significance with age by DESeq2 LRT (FDR < 1e-6).
(**A**) Complete piRNA mapping to TE Ovarian DESeq2 LRT Analysis with clusters as defined in **Fig. 2A**. (**B**) Complete piRNA mapping to TE Testicular DESeq2 LRT Analysis with clusters as defined in **Fig. 2A**.

Supplementary Table S6: List of piRNA targeted TE sequences with significant differential Z_{10} ping-pong scores with age by ANOVA (FDR < 0.05).

(**A**) TEs with significantly differential ping-pong Z_{10} scores in ovaries organized by clusters as defined in **Fig. 6D** (ANOVA FDR < 5%). (**B**) TEs with significantly differential ping-pong Z_{10} scores in testes organized by clusters as defined in **Fig. 6D** (ANOVA FDR < 5%).

Figure 1

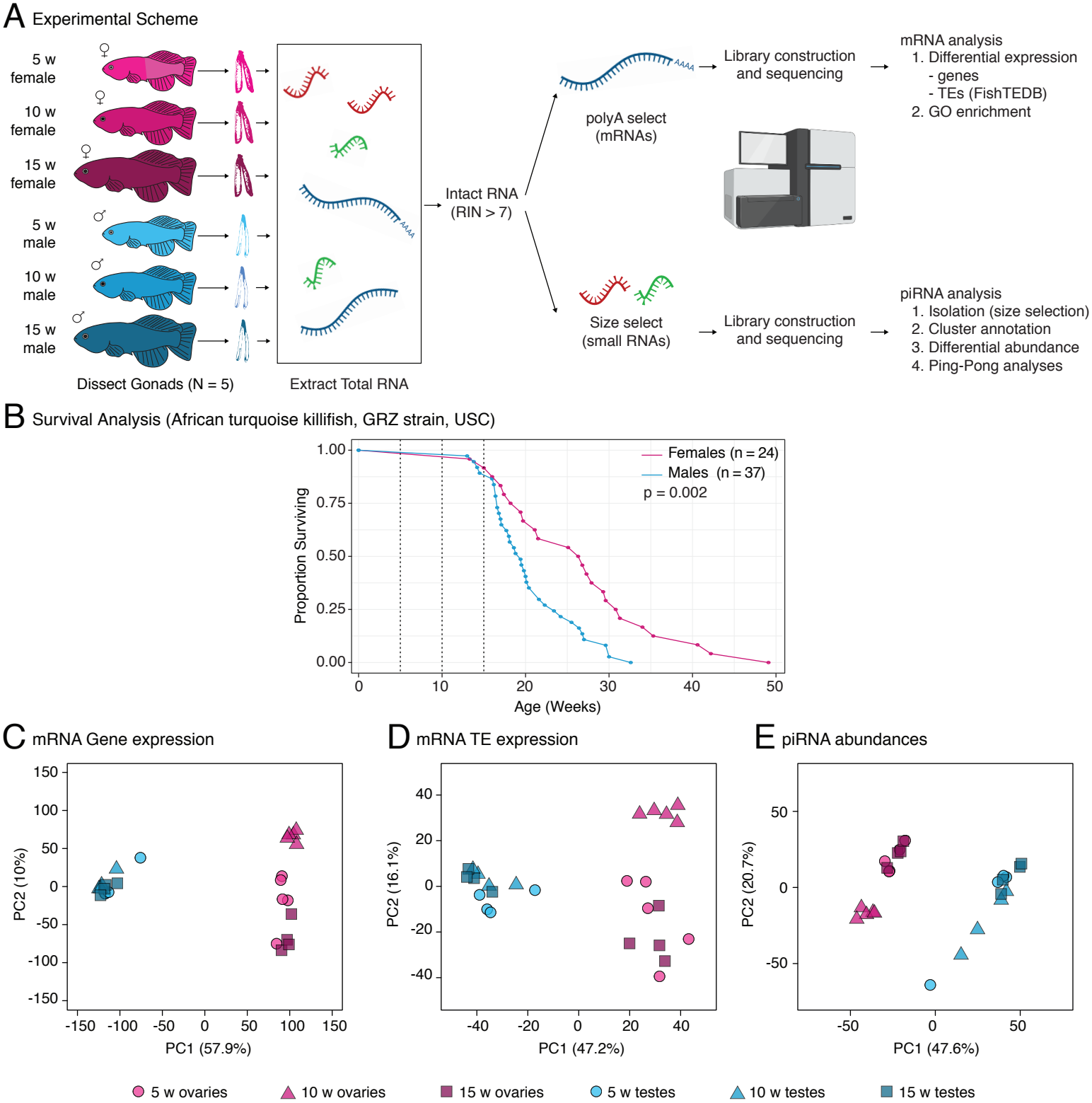
A Experimental Scheme
5 w female
10 w female
15 w female
5 w male
10 w male
15 w male
Dissect Gonads (N = 5)
Extract Total RNA
Intact RNA (RIN > 7)
polyA select (mRNAs)
Library construction and sequencing
mRNA analysis
1. Differential expression
- genes
- TEs (FishTEDB)
2. GO enrichment
Size select (small RNAs)
Library construction and sequencing
piRNA analysis
1. Isolation (size selection)
2. Cluster annotation
3. Differential abundance
4. Ping-Pong analyses
B Survival Analysis (African turquoise killifish, GRZ strain, USC)
Females (n = 24)
Males (n = 37)
p = 0.002
Proportion Surviving
Age (Weeks)
C mRNA Gene expression
PC2 (10%)
PC1 (57.9%)
D mRNA TE expression
PC2 (16.1%)
PC1 (47.2%)
E piRNA abundances
PC2 (20.7%)
PC1 (47.6%)
5 w ovaries
10 w ovaries
15 w ovaries
5 w testes
10 w testes
15 w testes

Figure 1. A study of gonadal aging in the naturally short-lived African turquoise killifish

(A) Experimental scheme for killifish gonad sequencing. Killifish gonads (N = 5) were dissected and total RNA was extracted. Only high quality RNA samples (RIN>7) were included for further processing (see **Fig. S1A**). Small RNA and mRNA RNA-seq libraries were derived from each total RNA sample and sequenced for downstream analyses. **(B)** Lifespan curve for female and male GRZ strain killifish at the USC Benayoun lab facility. GRZ females lived significantly longer than males ($p = 0.002$; log Rank test). Median lifespan of females: 26.55 weeks, males: 19.4 weeks. Vertical dotted lines: ages sampled in this study (5, 10, 15 weeks), chosen to represent aging before substantially decreased population survival. **(C-E)** Principal component analyses [PCAs] for **(C)** mRNA gene expression **(D)** TE expression and **(E)** TE-mapping piRNA abundance (see methods).

Figure 2

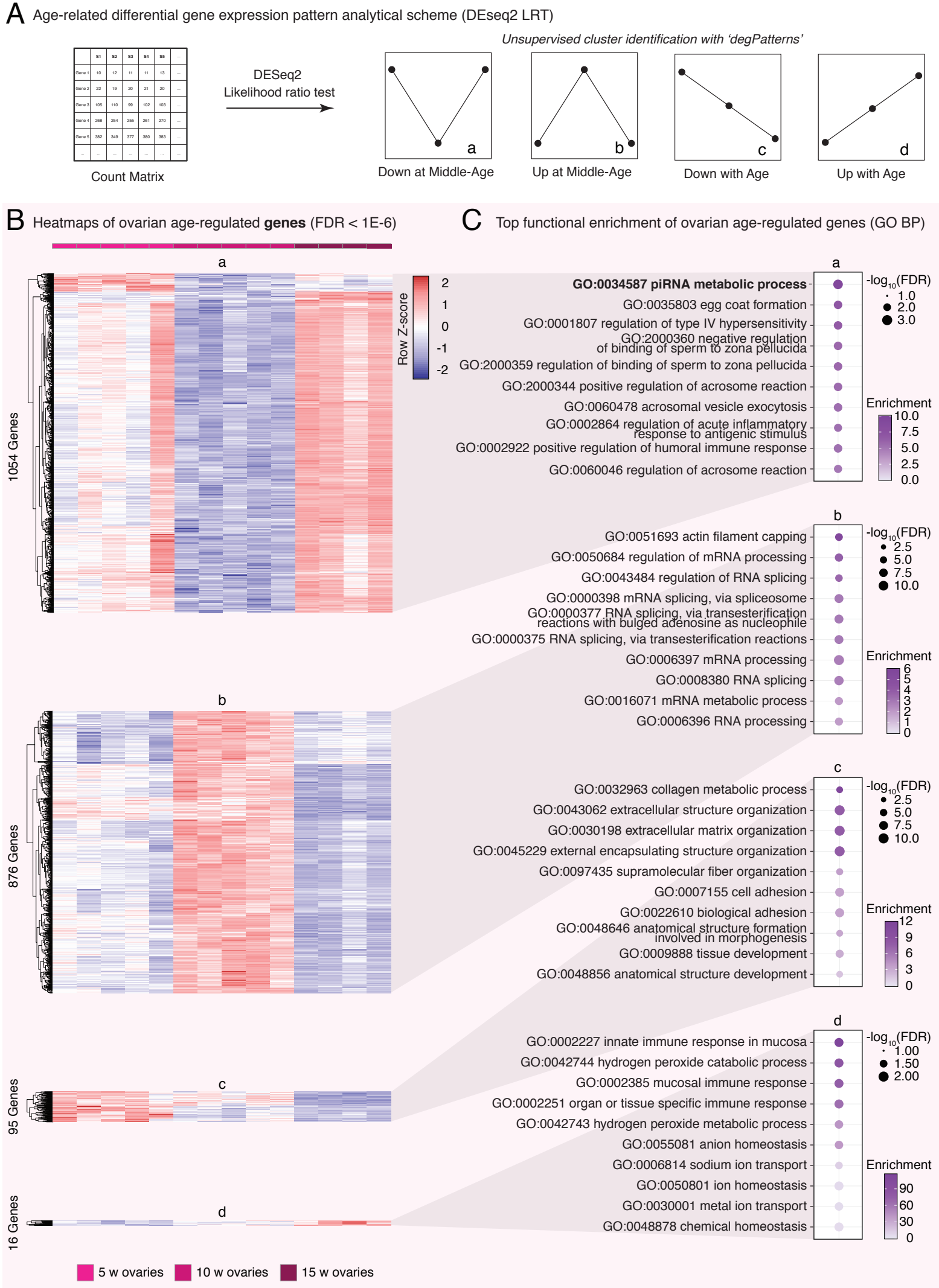
A
Age-related differential gene expression pattern analytical scheme (DEseq2 LRT)
Count Matrix
DESeq2
Likelihood ratio test
Unsupervised cluster identification with 'degPatterns'
a
Down at Middle-Age
b
Up at Middle-Age
c
Down with Age
d
Up with Age
B
Heatmaps of ovarian age-regulated genes (FDR < 1E-6)
1054 Genes
876 Genes
95 Genes
16 Genes
Row Z-score
2
1
0
-1
-2
5 w ovaries
10 w ovaries
15 w ovaries
C
Top functional enrichment of ovarian age-regulated genes (GO BP)
GO:0034587 piRNA metabolic process
GO:0035803 egg coat formation
GO:0001807 regulation of type IV hypersensitivity
GO:2000360 negative regulation of binding of sperm to zona pellucida
GO:2000359 regulation of binding of sperm to zona pellucida
GO:2000344 positive regulation of acrosome reaction
GO:0060478 acrosomal vesicle exocytosis
GO:0002864 regulation of acute inflammatory response to antigenic stimulus
GO:0002922 positive regulation of humoral immune response
GO:0060046 regulation of acrosome reaction
-log10(FDR)
1.0
2.0
3.0
Enrichment
10.0
7.5
5.0
2.5
0.0
GO:0051693 actin filament capping
GO:0050684 regulation of mRNA processing
GO:0043484 regulation of RNA splicing
GO:0000398 mRNA splicing, via spliceosome
GO:0000377 RNA splicing, via transesterification reactions with bulged adenosine as nucleophile
GO:0000375 RNA splicing, via transesterification reactions
GO:0006397 mRNA processing
GO:0008380 RNA splicing
GO:0016071 mRNA metabolic process
GO:0006396 RNA processing
-log10(FDR)
2.5
5.0
7.5
10.0
Enrichment
6
5
4
3
2
1
0
GO:0032963 collagen metabolic process
GO:0043062 extracellular structure organization
GO:0030198 extracellular matrix organization
GO:0045229 external encapsulating structure organization
GO:0097435 supramolecular fiber organization
GO:0007155 cell adhesion
GO:0022610 biological adhesion
GO:0048646 anatomical structure formation involved in morphogenesis
GO:0009888 tissue development
GO:0048856 anatomical structure development
-log10(FDR)
2.5
5.0
7.5
10.0
Enrichment
12
9
6
3
0
GO:0002227 innate immune response in mucosa
GO:0042744 hydrogen peroxide catabolic process
GO:0002385 mucosal immune response
GO:0002251 organ or tissue specific immune response
GO:0042743 hydrogen peroxide metabolic process
GO:0055081 anion homeostasis
GO:0006814 sodium ion transport
GO:0050801 ion homeostasis
GO:0030001 metal ion transport
GO:0048878 chemical homeostasis
-log10(FDR)
1.00
1.50
2.00
Enrichment
90
60
30
0

Figure 2. Differential gene expression analysis and GO Biological Process functional enrichment analysis with ovarian aging.

(A) Scheme used for differential gene expression [DGE] analysis used in this study. DGE was performed with DESeq2's likelihood ratio testing [LRT], which revealed 4 approximate groups of differentially expressed genes corresponding to expression (a) Down at Middle-Age, (b) Up at Middle-Age, (c) Down with Age and (d) Up with Age. **(B)** Heatmaps of gene expression for genes significantly regulated with age in aging killifish ovaries by DEseq2 LRT (FDR < 1e-6). Most differentially expressed genes transiently changed at middle-age. **(C)** Functional enrichment analysis for each gene cluster in **Fig. 2B**, showing the top 10 most significant GO "Biological Process" terms by 'GOstats' (FDR < 5%; see **Supplementary Table S3A** for complete list of enriched terms). The most significant term downregulated in middle-aged ovaries is "piRNA metabolic process" (bolded). FDR: False discovery rate. Enrichment: fold enrichment over background.

Figure 3

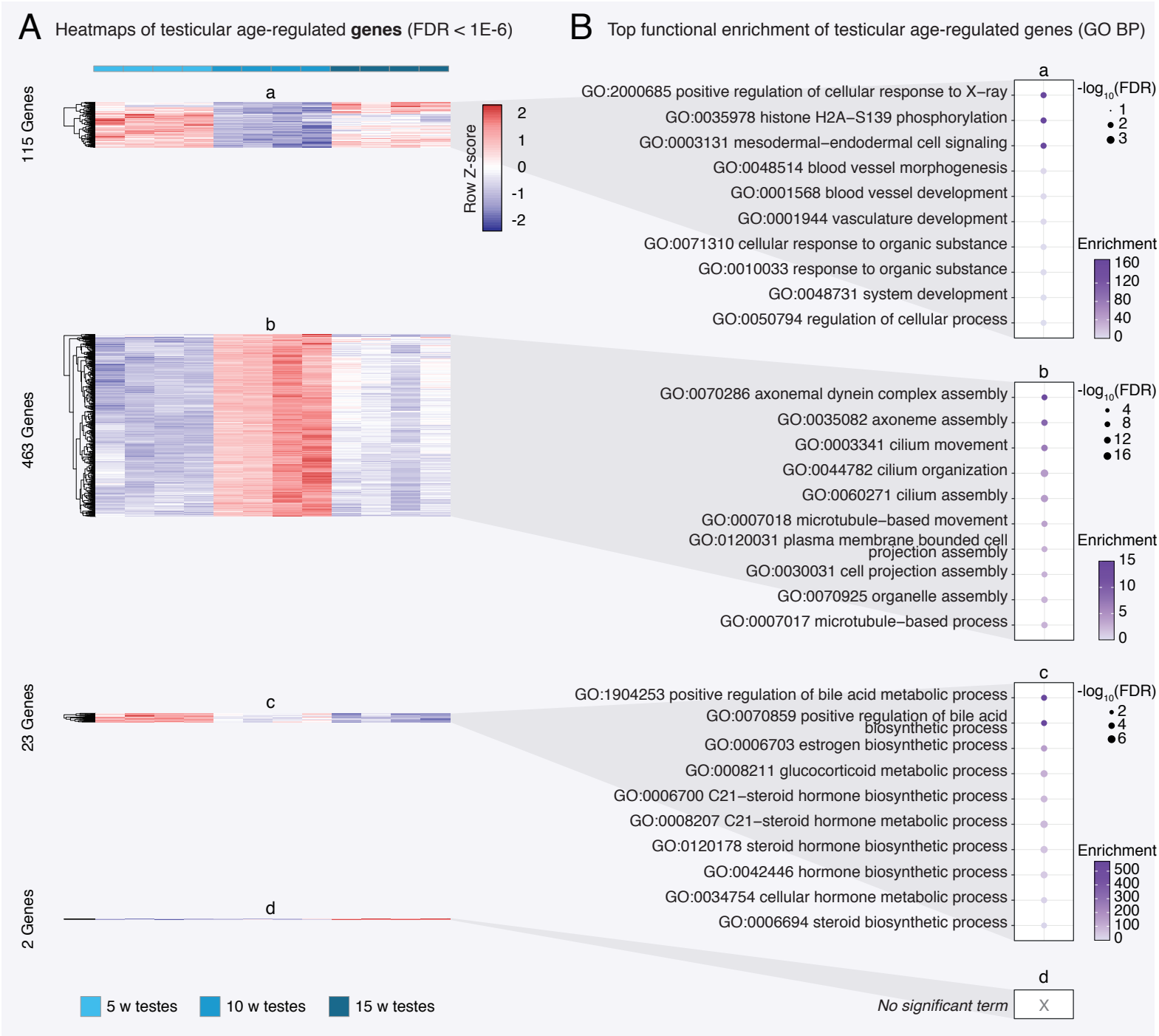
A
Heatmaps of testicular age-regulated genes (FDR < 1E-6)
B
Top functional enrichment of testicular age-regulated genes (GO BP)
115 Genes
463 Genes
23 Genes
2 Genes
a
b
c
d
Row Z-score
2
1
0
-1
-2
GO:2000685 positive regulation of cellular response to X−ray
GO:0035978 histone H2A−S139 phosphorylation
GO:0003131 mesodermal−endodermal cell signaling
GO:0048514 blood vessel morphogenesis
GO:0001568 blood vessel development
GO:0001944 vasculature development
GO:0071310 cellular response to organic substance
GO:0010033 response to organic substance
GO:0048731 system development
GO:0050794 regulation of cellular process
-log10(FDR)
1
2
3
Enrichment
160
120
80
40
0
GO:0070286 axonemal dynein complex assembly
GO:0035082 axoneme assembly
GO:0003341 cilium movement
GO:0044782 cilium organization
GO:0060271 cilium assembly
GO:0007018 microtubule−based movement
GO:0120031 plasma membrane bounded cell projection assembly
GO:0030031 cell projection assembly
GO:0070925 organelle assembly
GO:0007017 microtubule−based process
-log10(FDR)
4
8
12
16
Enrichment
15
10
5
0
GO:1904253 positive regulation of bile acid metabolic process
GO:0070859 positive regulation of bile acid biosynthetic process
GO:0006703 estrogen biosynthetic process
GO:0008211 glucocorticoid metabolic process
GO:0006700 C21−steroid hormone biosynthetic process
GO:0008207 C21−steroid hormone metabolic process
GO:0120178 steroid hormone biosynthetic process
GO:0042446 hormone biosynthetic process
GO:0034754 cellular hormone metabolic process
GO:0006694 steroid biosynthetic process
-log10(FDR)
2
4
6
Enrichment
500
400
300
200
100
0
No significant term
X
5 w testes
10 w testes
15 w testes

Figure 3. Differential gene expression and GO Biological Process functional enrichment analysis with testicular aging.

(A) Heatmaps of gene expression for genes significantly regulated with age in aging killifish testes by DEseq2 LRT (FDR < 1e-6). Groups correspond to those defined in **Fig. 2A**. Like ovaries, most differential gene expression in killifish testes occurs transiently at middle-age. **(B)** Functional enrichment analysis for each gene cluster shown in **Fig. 3A** showing the top 10 most significant GO "Biological Process" terms by 'GOstats' (FDR < 5%; see **Supplementary Table S3D** for complete list of enriched terms). Genes that are upregulated in middle-age testis are enriched for terms related to spermatogenesis. Note that cluster (d) (genes up with age) had too few genes to generate meaningful enrichment results. FDR: False discovery rate. Enrichment: fold enrichment over background.

Figure 4

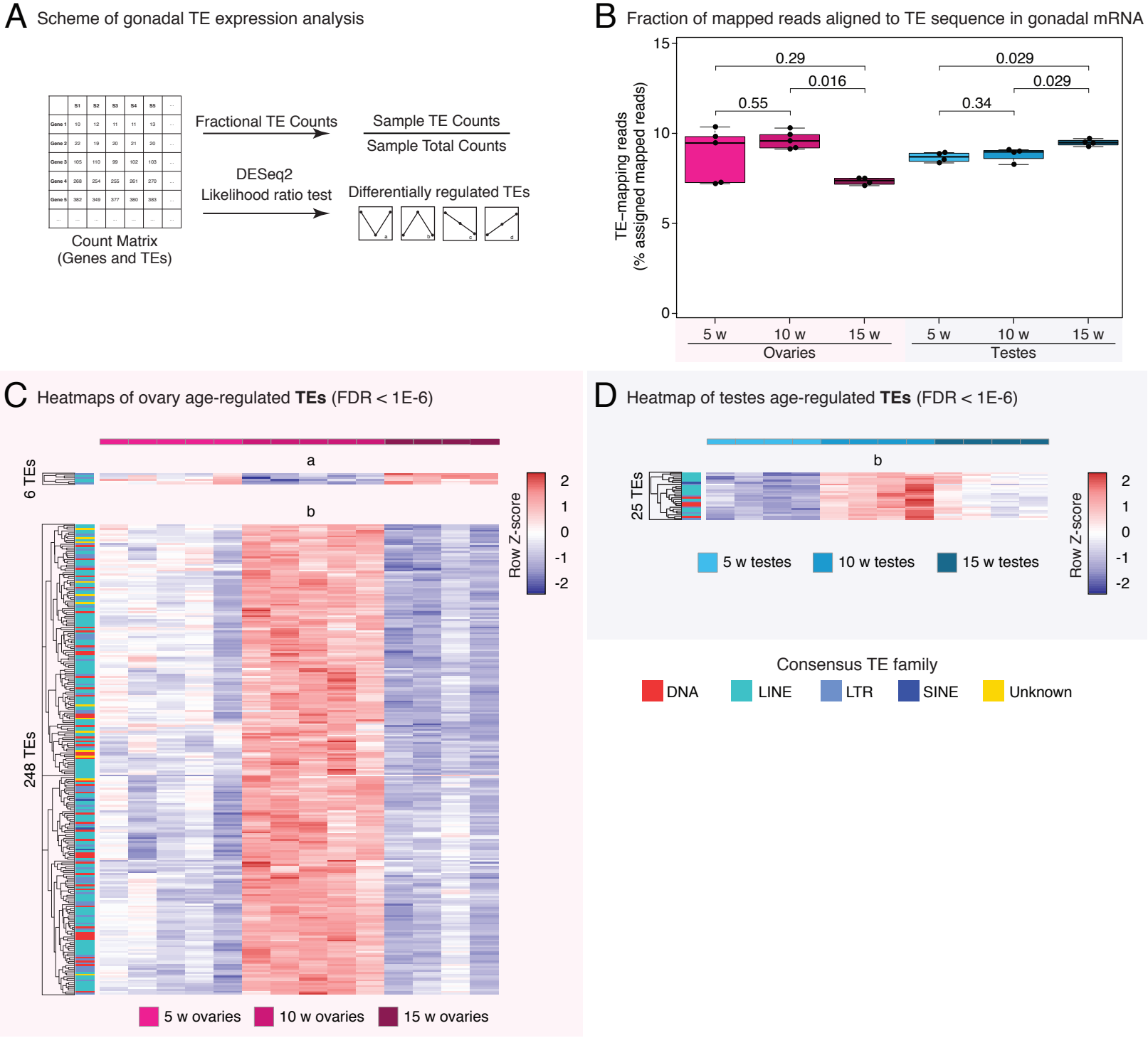
A Scheme of gonadal TE expression analysis
Count Matrix
(Genes and TEs)
Fractional TE Counts
Sample TE Counts
Sample Total Counts
DESeq2
Likelihood ratio test
Differentially regulated TEs
B Fraction of mapped reads aligned to TE sequence in gonadal mRNA
TE–mapping reads
(% assigned mapped reads)
0.29
0.016
0.55
0.029
0.029
0.34
5 w
10 w
15 w
Ovaries
Testes
C Heatmaps of ovary age-regulated TEs (FDR < 1E-6)
6 TEs
248 TEs
a
b
Row Z-score
5 w ovaries
10 w ovaries
15 w ovaries
D Heatmap of testes age-regulated TEs (FDR < 1E-6)
25 TEs
5 w testes
10 w testes
15 w testes
Consensus TE family
DNA
LINE
LTR
SINE
Unknown

Figure 4. TE expression dynamics in the aging turquoise killifish gonad.

(A) Experimental scheme for TE transcriptional analysis in aging gonads. Fractional TE counts were computed by counting the number of TE counts over total assigned mRNA-seq counts (genes and TEs). TE DGE was conducted in the same manner as the genic DGE analysis (see methods), and were labelled with the cluster nomenclature from **Fig. 2A**. **(B)** Proportion of assigned reads allocated to TEs from each mRNA-seq library for ovaries and testes. Significance in non-parametric Wilcoxon Rank Sum test. Note that old ovaries have significantly fewer proportional TE counts relative to middle-aged ovaries, and that testes seem to show a marginal increase in TE transcription with aging. **(C)** Heatmaps of mRNA expression for TEs significantly regulated with age in aging killifish ovaries by DEseq2 LRT (FDR < 1e-6). Each TE family is color-coded by row, revealing no obvious bias or enrichment for a specific TE type. **(D)** Heatmaps of mRNA expression for TEs significantly regulated with age in aging killifish testes by DEseq2 LRT (FDR < 1e-6). The only age differentially regulated TEs in the turquoise killifish testis are transiently upregulated at middle-age.

Figure 5

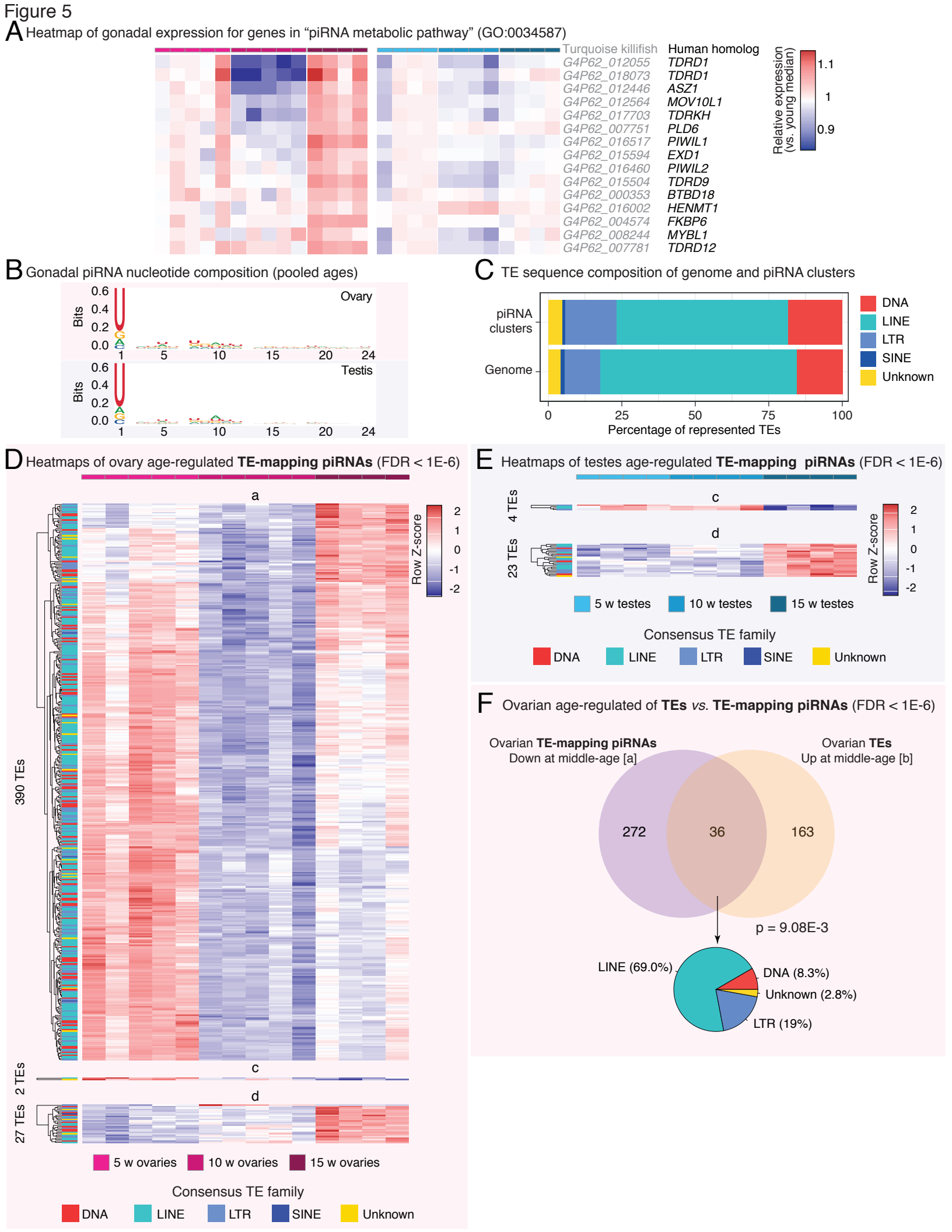
A
Heatmap of gonadal expression for genes in "piRNA metabolic pathway" (GO:0034587)
Turquoise killifish
Human homolog
G4P62_012055 TDRD1
G4P62_018073 TDRD1
G4P62_012446 ASZ1
G4P62_012564 MOV10L1
G4P62_017703 TDRKH
G4P62_007751 PLD6
G4P62_016517 PIWIL1
G4P62_015594 EXD1
G4P62_016460 PIWIL2
G4P62_015504 TDRD9
G4P62_000353 BTBD18
G4P62_016002 HENMT1
G4P62_004574 FKBP6
G4P62_008244 MYBL1
G4P62_007781 TDRD12
Relative expression (vs. young median)
1.1
1
0.9
B
Gonadal piRNA nucleotide composition (pooled ages)
Ovary
Testis
Bits
C
TE sequence composition of genome and piRNA clusters
piRNA clusters
Genome
DNA
LINE
LTR
SINE
Unknown
Percentage of represented TEs
D
Heatmaps of ovary age-regulated TE-mapping piRNAs (FDR < 1E-6)
390 TEs
2 TEs
27 TEs
Row Z-score
5 w ovaries
10 w ovaries
15 w ovaries
Consensus TE family
E
Heatmaps of testes age-regulated TE-mapping piRNAs (FDR < 1E-6)
4 TEs
23 TEs
5 w testes
10 w testes
15 w testes
F
Ovarian age-regulated of TEs vs. TE-mapping piRNAs (FDR < 1E-6)
Ovarian TE-mapping piRNAs
Down at middle-age [a]
Ovarian TEs
Up at middle-age [b]
272
36
163
p = 9.08E-3
LINE (69.0%)
DNA (8.3%)
Unknown (2.8%)
LTR (19%)

Figure 5. PIWI pathway activity and piRNA abundance characterization in aging turquoise killifish gonads.

(A) Heatmaps of normalized gene expression from ovaries and testes with aging in the GO "piRNA metabolic pathway" term. Killifish gene names and their best human homologs are indicated for each row. Rows were normalized by the median expression level in the cognate young gonad, so as to facilitate visualization of age-related changes. Genes involved in this pathway tend to be significantly downregulated in middle-aged ovaries (see **Fig. 2C**). **(B)** Sequence logo plots of piRNA nucleotide composition from ovaries and testes, using data for each gonad type pooled across ages and replicates. As expected for piRNAs, killifish piRNAs show a strong position 1-U bias. There is also a slight bias for Adenine at position 10, consistent with active ping-pong biogenesis in killifish gonads. **(C)** Stacked barplots depicting the TE family composition of piRNA clusters and the killifish genome, as a percentage of identified elements. The piRNA cluster TE composition is broadly reflective of the TE composition of the genome. **(D)** Heatmaps of TE-targeted piRNA abundance for TEs significantly regulated with age in aging killifish ovaries by DEseq2 LRT (FDR < 1e-6). TE family is color-coded for each row. In ovaries, most differentially piRNA-targeted TEs show a decrease of piRNA counts at middle-age. **(E)** Heatmaps of TE-targeted piRNA abundance for TEs significantly regulated with age in aging killifish testes by DEseq2 LRT (FDR < 1e-6). **(F)** Venn diagram of the overlap between TE_mapping piRNAs significantly <u>up</u>regulated in middle-age ovaries (see **Fig. 5D**; pattern a) and TEs that are significantly <u>down</u>regulated in middle-age ovaries (see **Fig. 4C**; pattern b). Significance for the overlap being larger than expected by chance was calculated using Fisher's exact test, compared to TEs detected in both analyses. A pie chart of the composition of "consistent" TEs is also reported.

Figure 6

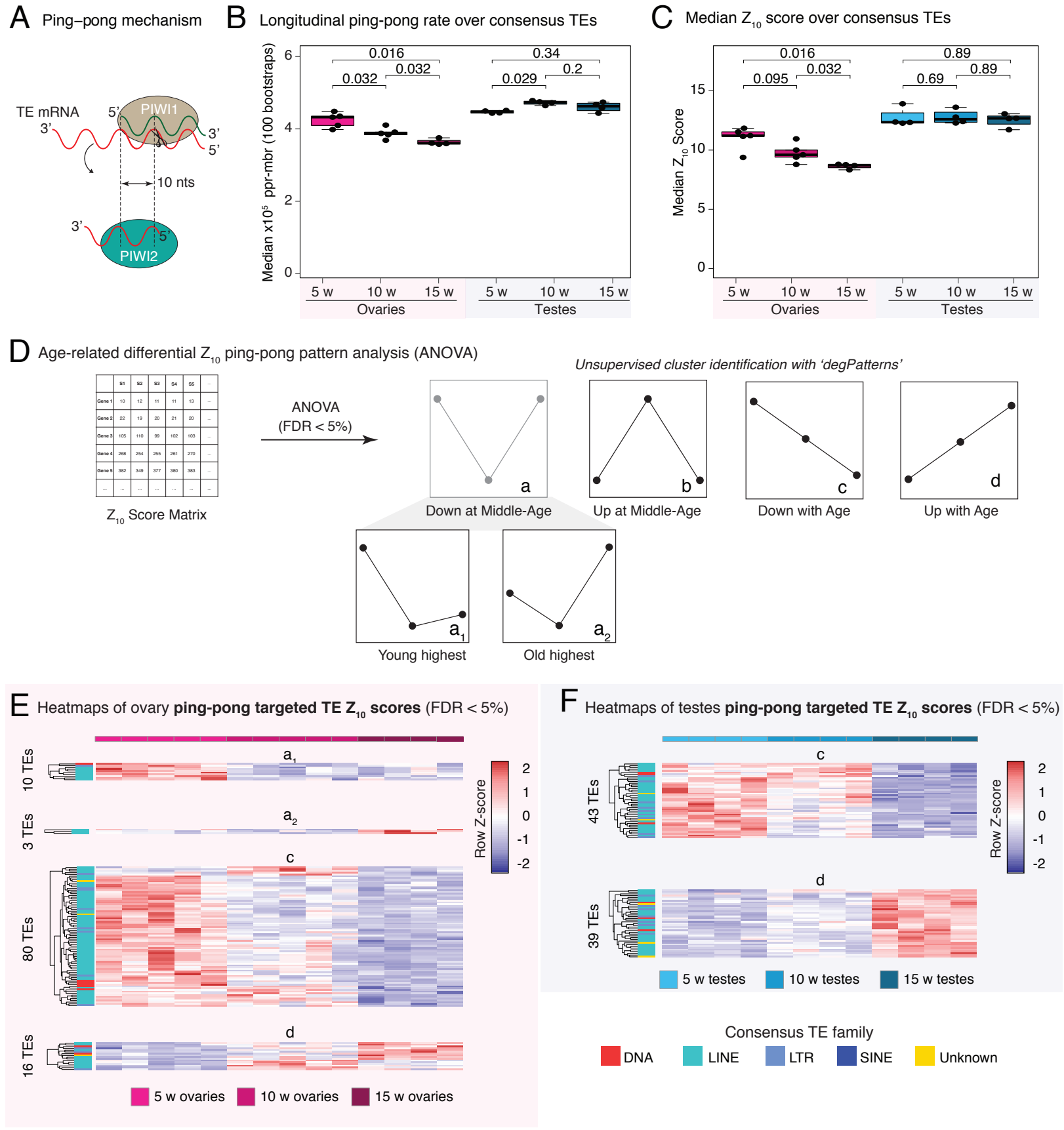
A Ping–pong mechanism
TE mRNA
5'
3'
PIWI1
3'
5'
10 nts
3'
5'
PIWI2
B Longitudinal ping-pong rate over consensus TEs
Median x10^5 ppr-mbr (100 bootstraps)
0.016
0.032
0.032
0.34
0.029
0.2
5 w
10 w
15 w
Ovaries
Testes
C Median Z10 score over consensus TEs
Median Z10 Score
0.016
0.095
0.032
0.89
0.69
0.89
5 w
10 w
15 w
Ovaries
Testes
D Age-related differential Z10 ping-pong pattern analysis (ANOVA)
Z10 Score Matrix
ANOVA
(FDR < 5%)
Unsupervised cluster identification with 'degPatterns'
a
Down at Middle-Age
b
Up at Middle-Age
c
Down with Age
d
Up with Age
a1
Young highest
a2
Old highest
E Heatmaps of ovary ping-pong targeted TE Z10 scores (FDR < 5%)
10 TEs
3 TEs
80 TEs
16 TEs
a1
a2
c
d
Row Z-score
5 w ovaries
10 w ovaries
15 w ovaries
F Heatmaps of testes ping-pong targeted TE Z10 scores (FDR < 5%)
43 TEs
39 TEs
c
d
Row Z-score
5 w testes
10 w testes
15 w testes
Consensus TE family
DNA
LINE
LTR
SINE
Unknown

Figure 6. Analysis of ping-pong biogenesis in aging turquoise killifish gonads.

(A) Explanatory diagram of ping-pong biogenesis. PIWI1 (the PIWI protein loaded with 'primary' piRNAs complementary to TEs) binds to and cleaves a TE mRNA species. The cleaved TE mRNA is loaded into PIWI2 (the PIWI protein loaded with cleaved TE fragments, or 'TE-derived secondary' piRNAs). PIWI proteins always cleave their targets 10 basepairs from the 5' end of the piRNA. This mechanism, known as ping-pong biogenesis, will generate a preponderance of complementary piRNAs with a 10 basepair overlap, the detection of which is the basis of the assays shown in **Fig. 6B-F**. **(B)** Boxplot showing the median frequency of 10 basepair overlaps for 1 million piRNA reads over 100 bootstraps per biological sample (ppr-mbr: Ping-Pong Reads per Million Bootstrapped Reads,) as generated by PPmeter. Age groups within each sex were compared using the non-parametric Wilcoxon rank sum test. **(C)** Boxplot showing median Z_{10} scores over consensus TEs for each biological sample. Z_{10} scores are an alternative measure of ping-pong. Non-parametric Wilcoxon Rank Sum tests were used to test for significant differences between age groups. **(D)** Schematic for analysis of differential Z_{10} score patterns with gonadal aging. Z_{10} scores were generated for each consensus TE sequence in FishTEDB in each biological sample. An ANOVA test was run to detect any significant differences in Z_{10} score between age groups within each sex (FDR < 5%). Significant TEs were assigned to groups based on expression dynamics that align to the broad groups defined in **Fig. 2A**, with the detection of 2 new subgroups showing minimal expression at middle-age (a_1 and a_2), with highest Z_{10} scores in the young samples and old samples, respectively. **(E)** Heatmaps of differential Z_{10} scores with age in aging killifish ovaries by ANOVA (FDR < 5%). **(F)** Heatmaps of differential Z_{10} scores with age in aging killifish testes by ANOVA (FDR < 5%). A roughly equivalent amount of consensus TE sequences show linear up- and downregulation with age. The cognate TE family is color-coded by row, and does not reveal any specific bias.

Figure S1

A

Datasets generated in this study	Ovary	Testes	Total
mRNA-seq	5,5,4 (14)	4,4,4 (12)	26
small RNA-seq	5,5,4 (14)	4,4,4 (12)	26

52 datasets

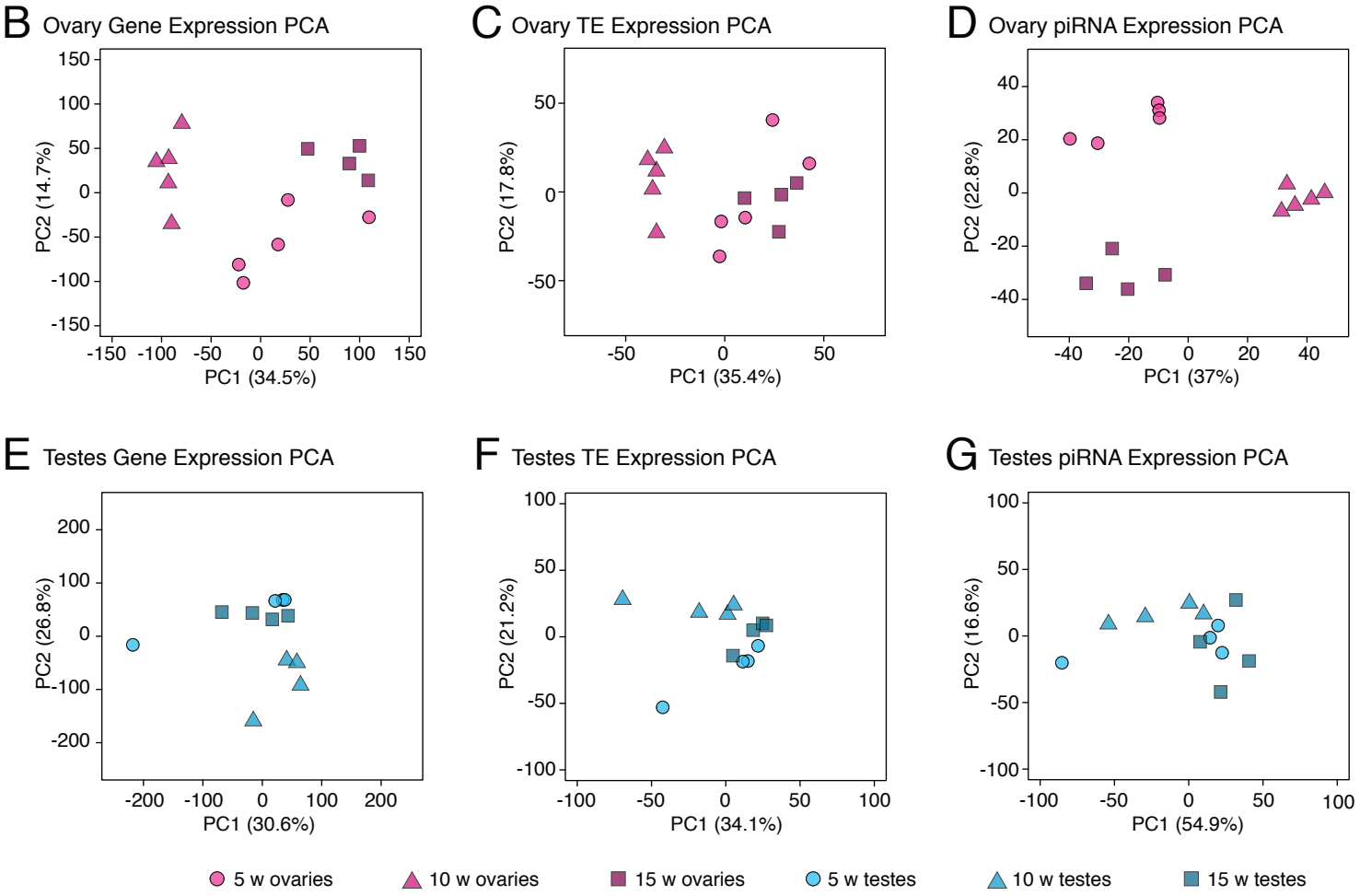

Figure S1. Global Characterization of aging turquoise killifish gonadal Dataset.

(A) Description of datasets generated in this study. A total of 26 RNA-seq and 26 small RNA-seq datasets were generated from ovary and testes from ages 5, 10, and 15 weeks old. **(B-G)** PCA plots of (B) ovarian gene expression, (C) ovarian TE expression, (D) ovarian TE-targeted piRNA abundance, (E) testicular gene expression, (F) testicular TE expression, (G) testicular TE-targeted piRNA abundance.

Figure S2

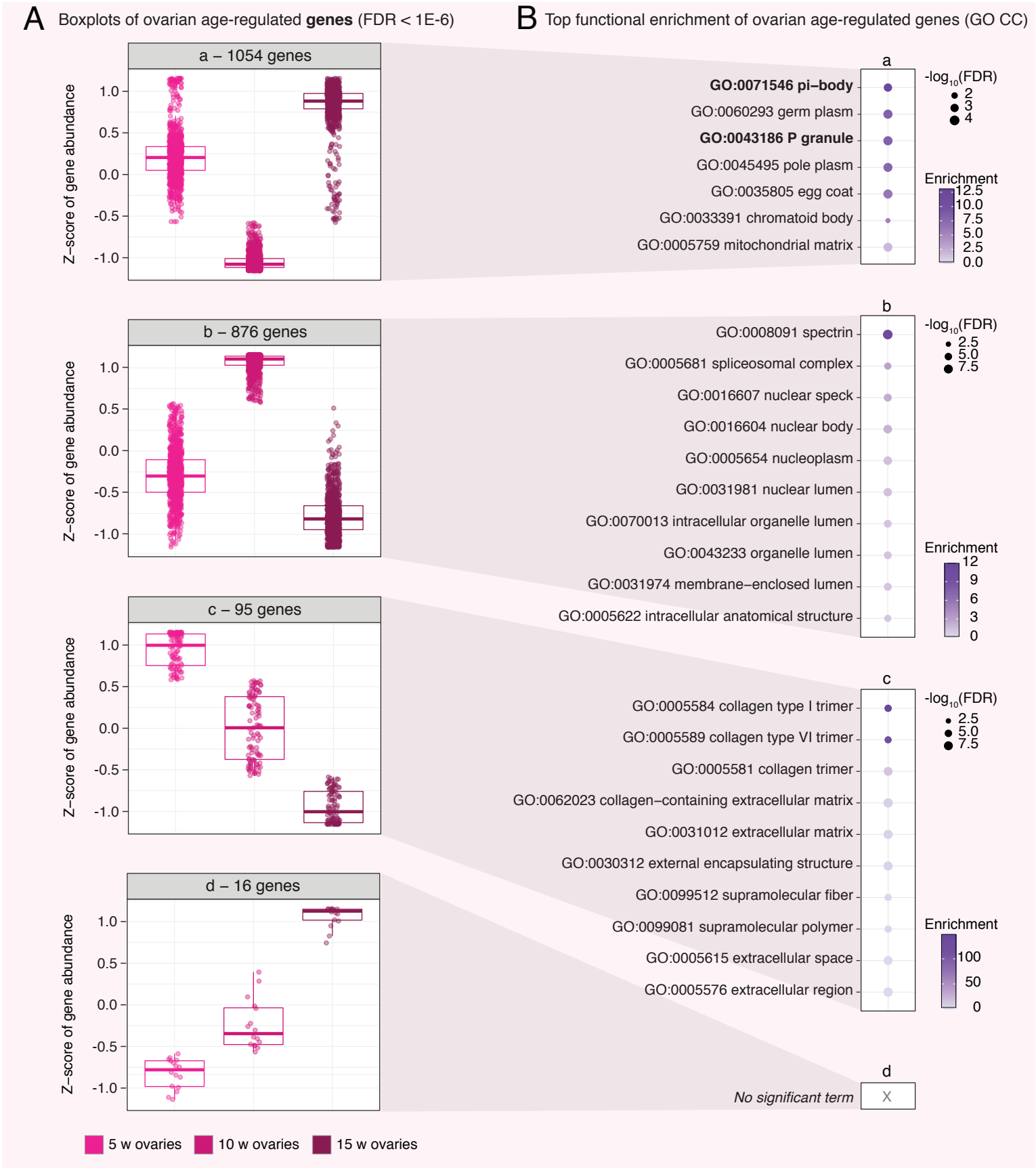
A
Boxplots of ovarian age-regulated genes (FDR < 1E-6)
B
Top functional enrichment of ovarian age-regulated genes (GO CC)
a – 1054 genes
b – 876 genes
c – 95 genes
d – 16 genes
Z–score of gene abundance
1.0
0.5
0.0
-0.5
-1.0
a
GO:0071546 pi–body
GO:0060293 germ plasm
GO:0043186 P granule
GO:0045495 pole plasm
GO:0035805 egg coat
GO:0033391 chromatoid body
GO:0005759 mitochondrial matrix
-log10(FDR)
2
3
4
Enrichment
12.5
10.0
7.5
5.0
2.5
0.0
b
GO:0008091 spectrin
GO:0005681 spliceosomal complex
GO:0016607 nuclear speck
GO:0016604 nuclear body
GO:0005654 nucleoplasm
GO:0031981 nuclear lumen
GO:0070013 intracellular organelle lumen
GO:0043233 organelle lumen
GO:0031974 membrane–enclosed lumen
GO:0005622 intracellular anatomical structure
-log10(FDR)
2.5
5.0
7.5
Enrichment
12
9
6
3
0
c
GO:0005584 collagen type I trimer
GO:0005589 collagen type VI trimer
GO:0005581 collagen trimer
GO:0062023 collagen–containing extracellular matrix
GO:0031012 extracellular matrix
GO:0030312 external encapsulating structure
GO:0099512 supramolecular fiber
GO:0099081 supramolecular polymer
GO:0005615 extracellular space
GO:0005576 extracellular region
-log10(FDR)
2.5
5.0
7.5
Enrichment
100
50
0
d
No significant term
X
5 w ovaries
10 w ovaries
15 w ovaries

Figure S2. Differential gene expression analysis and GO 'cellular component' enrichment analysis in aging turquoise killifish ovaries.

(A) Boxplots of differentially expressed gene expression groups in ovaries by DEseq2 LRT (FDR < 1e-6). Each dot represents the expression level of a significantly differentially expressed gene in each group normalized by Z-score for ease of group-to-group comparison. **(B)** Top 10 GO "Cellular Component" terms enriched in each associated cluster according to 'GOstats' (FDR < 5%; see **Supplementary Table S3B** for the complete list of enriched terms). Terms down at middle-age related to the PIWI pathway include "pi-body" and "P granule" terms. Patterns are labelled according to **Fig. 2A**. FDR: False discovery rate. Enrichment: fold enrichment over background.

Figure S3

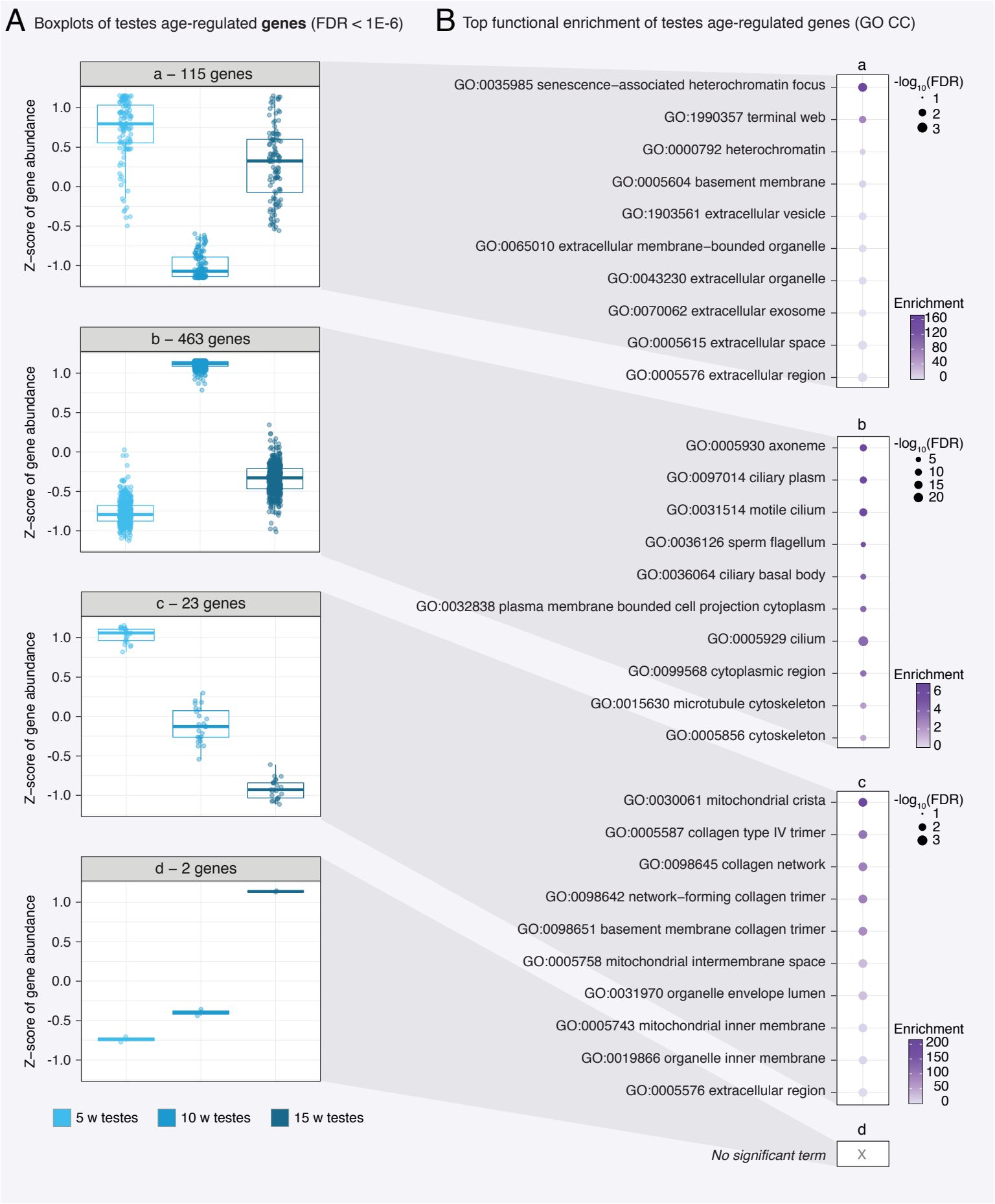
A Boxplots of testes age-regulated genes (FDR < 1E-6)
B Top functional enrichment of testes age-regulated genes (GO CC)
a – 115 genes
b – 463 genes
c – 23 genes
d – 2 genes
Z–score of gene abundance
1.0
0.5
0.0
-0.5
-1.0
5 w testes
10 w testes
15 w testes
a
GO:0035985 senescence–associated heterochromatin focus
GO:1990357 terminal web
GO:0000792 heterochromatin
GO:0005604 basement membrane
GO:1903561 extracellular vesicle
GO:0065010 extracellular membrane–bounded organelle
GO:0043230 extracellular organelle
GO:0070062 extracellular exosome
GO:0005615 extracellular space
GO:0005576 extracellular region
-log10(FDR)
1
2
3
Enrichment
160
120
80
40
0
b
GO:0005930 axoneme
GO:0097014 ciliary plasm
GO:0031514 motile cilium
GO:0036126 sperm flagellum
GO:0036064 ciliary basal body
GO:0032838 plasma membrane bounded cell projection cytoplasm
GO:0005929 cilium
GO:0099568 cytoplasmic region
GO:0015630 microtubule cytoskeleton
GO:0005856 cytoskeleton
-log10(FDR)
5
10
15
20
Enrichment
6
4
2
0
c
GO:0030061 mitochondrial crista
GO:0005587 collagen type IV trimer
GO:0098645 collagen network
GO:0098642 network–forming collagen trimer
GO:0098651 basement membrane collagen trimer
GO:0005758 mitochondrial intermembrane space
GO:0031970 organelle envelope lumen
GO:0005743 mitochondrial inner membrane
GO:0019866 organelle inner membrane
GO:0005576 extracellular region
-log10(FDR)
1
2
3
Enrichment
200
150
100
50
0
d
No significant term
X

Figure S3. Differential gene expression analysis and GO 'cellular component' enrichment analysis in aging turquoise killifish testes.

(A) Boxplots of differentially expressed gene expression groups in testes by DEseq2 LRT (FDR < 1e-6). Each dot represents the expression level of a significantly differentially expressed gene in each group normalized by Z-score for ease of group-to-group comparison. **(B)** Top 10 GO "Cellular Component" terms enriched in each associated cluster according to 'GOstats' (FDR < 5%; see **Supplementary Table S3E** for the complete list of enriched terms). Most terms enriched at middle-age are related to spermatogenesis. Patterns are labelled according to **Fig. 2A**. FDR: False discovery rate. Enrichment: fold enrichment over background.

Figure S4

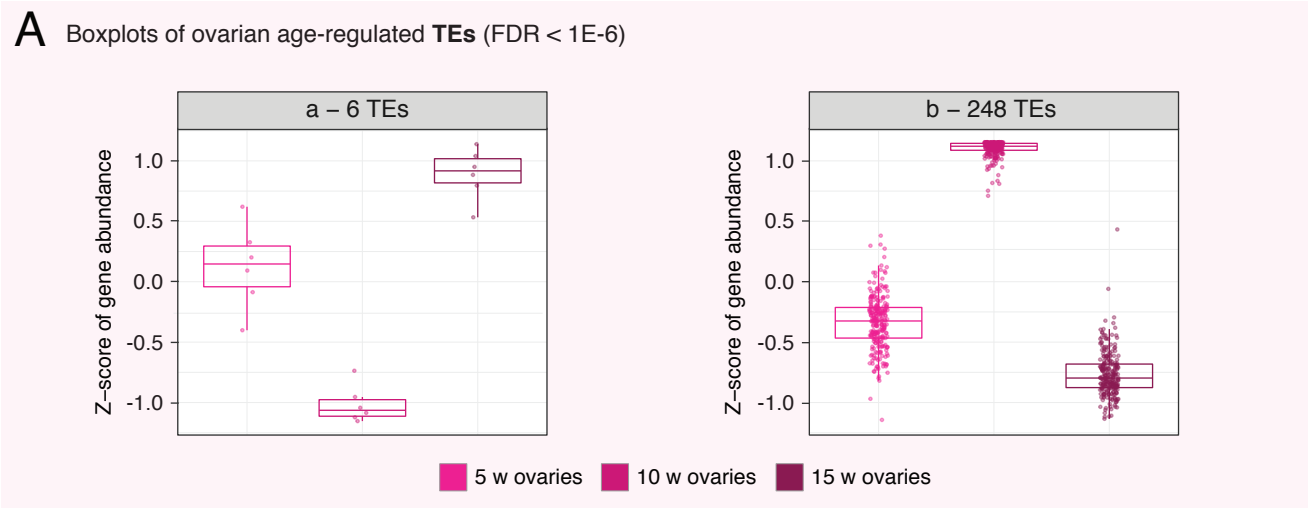
A
Boxplots of ovarian age-regulated **TEs** (FDR < 1E-6)
a – 6 TEs
b – 248 TEs
Z−score of gene abundance
1.0
0.5
0.0
-0.5
-1.0
5 w ovaries
10 w ovaries
15 w ovaries

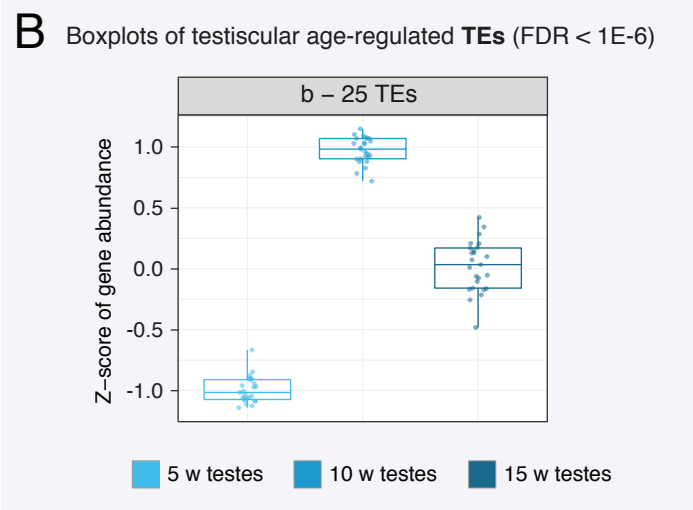
B
Boxplots of testiscular age-regulated **TEs** (FDR < 1E-6)
b – 25 TEs
Z−score of gene abundance
1.0
0.5
0.0
-0.5
-1.0
5 w testes
10 w testes
15 w testes

Figure S4. TE expression dynamics in the gonads of aging turquoise killifish.

(A) Boxplots of significantly differentially expressed TE clusters in ovaries by DEseq2 LRT (FDR < 1e-6). **(B)** Boxplot of the differentially expressed TE clusters in testes by DEseq2 LRT (FDR < 1e-6). Each dot represents the expression level of a significantly differentially expressed gene in each group normalized by Z-score for ease of group-to-group comparison. Patterns are labelled according to **Fig. 2A**.

Figure S5

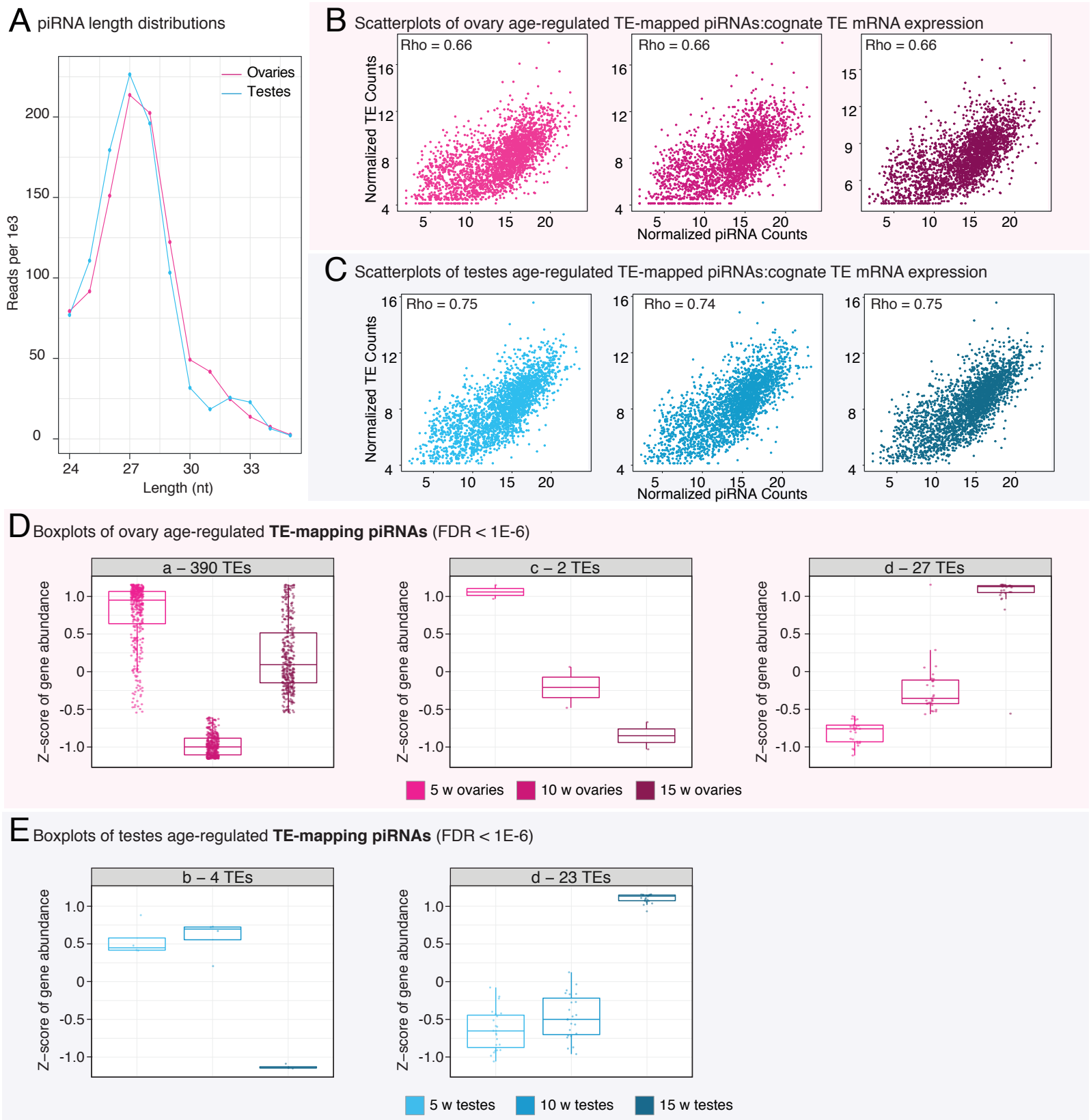
A piRNA length distributions
Ovaries
Testes
Reads per 1e3
Length (nt)
B Scatterplots of ovary age-regulated TE-mapped piRNAs:cognate TE mRNA expression
Rho = 0.66
Rho = 0.66
Rho = 0.66
Normalized TE Counts
Normalized piRNA Counts
C Scatterplots of testes age-regulated TE-mapped piRNAs:cognate TE mRNA expression
Rho = 0.75
Rho = 0.74
Rho = 0.75
Normalized TE Counts
Normalized piRNA Counts
D Boxplots of ovary age-regulated **TE-mapping piRNAs** (FDR < 1E-6)
a – 390 TEs
c – 2 TEs
d – 27 TEs
Z–score of gene abundance
5 w ovaries
10 w ovaries
15 w ovaries
E Boxplots of testes age-regulated **TE-mapping piRNAs** (FDR < 1E-6)
b – 4 TEs
d – 23 TEs
Z–score of gene abundance
5 w testes
10 w testes
15 w testes

Figure S5. piRNA characterization and regulation in aging turquoise killifish gonads.
(A) piRNA length distribution shown by sex, after computational filtering of small RNAs 24-35 bp. Both ovaries and testes have similar piRNA length profiles, with the majority of detected species at ~27bp. **(B)** Scatterplots of young, middle-aged, and old killifish ovaries normalized TE expression *vs.* piRNA counts assigned to the same cognate consensus TE sequence. There is a strong Spearman rank correlation Rho in all ovarian age groups (Rho = 0.66; significance of correlation test: $p < 2.2e-16$), indicating that piRNAs are produced sustainably throughout life in response to expressed TEs. **(C)** Scatterplots of young, middle-aged, and old killifish testes normalized TE expression *vs.* piRNA counts assigned to the same cognate consensus TE sequence . There is a slightly higher Spearman rank correlation in testes than ovaries (Rho = 0.74-0.75; significance of correlation test: $p < 2.2e-16$), likely reflecting a larger proportion of germ cells in testicular tissue. Rho: Spearman rank correlation value. **(D)** Boxplots of differentially piRNA-mapped groups of TEs in ovaries, by DEseq2 LRT (FDR < 1e-6), using the grouping arrangement defined in **Fig. 2A**. **(E)** Boxplots of differentially piRNA-mapped groups of TEs in testes by DEseq2 LRT (FDR < 1e-6).

Figure S6

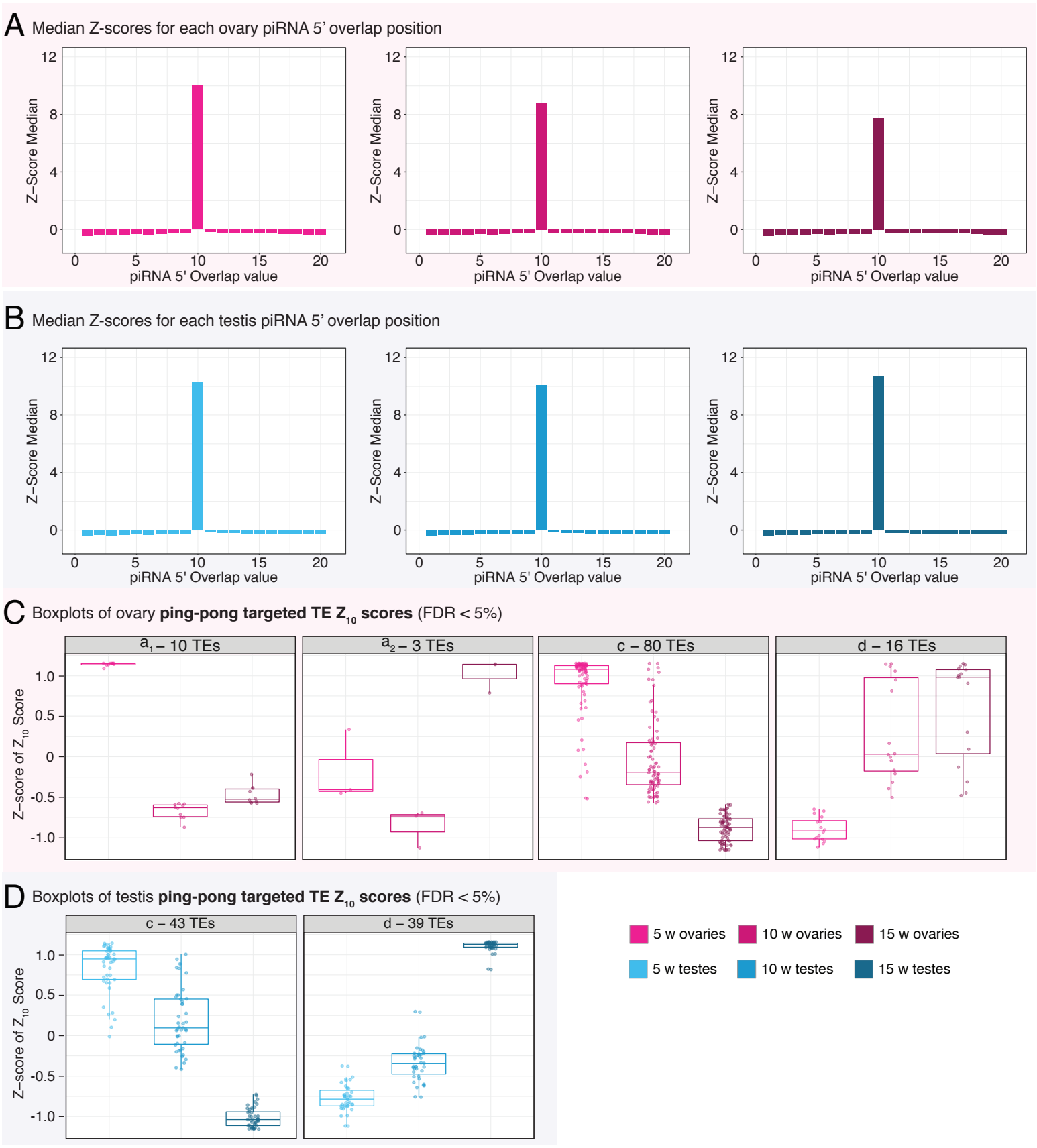
A Median Z-scores for each ovary piRNA 5' overlap position
Z−Score Median
piRNA 5' Overlap value
B Median Z-scores for each testis piRNA 5' overlap position
Z−Score Median
piRNA 5' Overlap value
C Boxplots of ovary ping-pong targeted TE Z10 scores (FDR < 5%)
a1 – 10 TEs
a2 – 3 TEs
c – 80 TEs
d – 16 TEs
Z−score of Z10 Score
D Boxplots of testis ping-pong targeted TE Z10 scores (FDR < 5%)
c – 43 TEs
d – 39 TEs
Z−score of Z10 Score
5 w ovaries
10 w ovaries
15 w ovaries
5 w testes
10 w testes
15 w testes

Figure S6. Analysis of ping-pong biogenesis signatures in aging turquoise killifish gonads (continued).

(A) Median Z_i-scores in ovaries grouped by age measured for each position within a 20 basepair window as summarized for position 10 in **Fig. 6C**. The highest Z_i-score occurs at position 10 (corresponding to the Z_{10} value), indicating that ping-pong is occurring at all ages. **(B)** Median Z_i-scores in testes grouped by age measured for each position within a 20 basepair window. Like the ovarian samples, the highest Z_{10}-score occurs at position 10 indicating ping-pong activity. **(C)** Boxplots of differential Z_{10} scores of TEs grouped into patterns in ovaries (patterns defined in **Fig. 6D**). Each dot is the Z-normalized Z_{10} score per age group. **(D)** Boxplots of differential Z_{10} scores of TEs grouped into clusters in testes. Each dot is the Z-normalized Z_{10} score per age group.